Tampere University

Aki Pöyhönen

MODELLING 5G NETWORK WITH NETWORK PLANNING TOOL AND VERIFYING RESULTS WITH FIELD MEASUREMENTS

Master of Science Thesis
Faculty of Information Technology and Communication Science
Examiners: Dr. Joonas Säe
Prof. Jukka Lempiäinen
October 2022

ABSTRACT

Aki Pöyhönen: Modelling 5G network with network planning tool and verifying results with field measurements
Master of Science Thesis
Tampere University
Master's Degree Programme in Electrical Engineering
October 2022

Wireless communications systems aim to achieve higher throughput, smaller latency, and better reliability for ever-growing demand. This creates challenges since radio resources are limited and a need for new technologies to achieve these demands is imminent. The ability to accurately model and simulate wireless networks becomes crucial to efficient radio network planning and optimization. Precise radio network models that generate accurate simulation results can be utilized to better understand and overcome the bottlenecks of designated radio networks.

In this thesis work the fifth generation (5G) Radio Access Network (RAN) model is built by using the radio network planning tool ASSET Radio and each part of the model is introduced along with RAN topology. The relevant selected system-level simulation results of the 5G RAN model are compared to field measurement results from equivalent real-life 5G RAN.

The differences and the similarities of the results between system-level simulation and field measurements are analyzed and the root causes for those results are made known. The main objective of this thesis work is to better understand key factors that impact the system-level simulation and the field measurement results of the 5G network. Furthermore, the key findings of this thesis work can be used to create more accurate 5G network models and overcome the challenges related to the 5G field measurements.

The results from this thesis work indicate that the radio network planning tool ASSET Radio can build an accurate 5G RAN model, which produces similar results to the results obtained from field measurements. With enough information of a designated 5G RAN, relatively precise results can be produced with ASSET Radio's system-level simulation and depending on the required level of accuracy, potentially leaving the field measurements unnecessary.

Keywords: 5G NR, 5G modelling , 5G simulation , 5G field measurements

TIIVISTELMÄ

Aki Pöyhönen: 5G-verkon mallintaminen verkkosunnittelutyökalua käyttäen ja tuloksien todentaminen kenttämittauksilla
Diplomityö
Tampereen yliopisto
Sähkötekniikan DI-tutkinto-ohjelma
Lokakuu 2022

Matkapuhelinverkot pyrkivät saavuttamaan korkeampaa bittinopeutta, pienempää viivettä ja parempaa toimintavarmuutta jatkuvasti kasvavaan kysyntään. Tämä luo haasteita, sillä radio resurssit ovat rajalliset ja tarve uusille teknologioille on ilmeinen, jotta nämä vaatimukset voidaan täyttää. Kyky mallintaa ja simuloida matkapuhelinverkkoja tarkasti on olennainen osa, jotta tehokasta matkapuhelinverkkojen suunnittelua ja optimimointi voi tehdä. Todenmukaisilla simulointituloksilla, joita tarkasta matkapuhelinverkon mallista saa, voidaan käyttää hyödyksi ymmärtämään kyseistä verkkoa paremmin ja selvittämään sen verkon mahdolliset pullonkaulat.

Tässä diplomityössä rakennettiin viidennen sukupolven (5G) radioliityntäverkon malli, jossa mallin jokainen osa on esitelty kuten myös radioliityntäverkon topologia käyttäen radioverkkojen suunnittelutyökalua ASSET Radiota. Radioliityntäverkon mallin oleellisimpia järjestelmätason simulointituloksia verrattiin vastaavan todellisen radioliityntäverkon mittaustuloksiin.

Järjestelmätason simulointituloksien ja mittaustuloksien välisiä eroja ja samankaltaisuuksia analysoidaan ja tuodaan esille pääsyitä, jotka johtivat näihin tuloksiin. Tämän diplomityön päätavoite on auttaa ymmärtämään paremmin päätekijöitä, jotka vaikuttavat 5G verkon simulointituloksiin ja mittaustuloksiin. Lisäksi tämän diplomityön päälöytöjen avulla voidaan rakentaa tarkempia 5G verkon malleja ja selvittämään haasteet, joita 5G verkon mittauksissa esiintyy.

Tämän diplomityön tulokset viittaavat siihen, että radioverkkojen suunnittelutyökalu ASSET Radio:lla on kykenevyys rakentaa tarkka 5G radioliityntäverkon malli, joka tuottaa samankaltaisia tuloksia kuin mittauksista saadut tulokset. Riittävällä tiedolla määrätystä 5G radioliityntäverkosta voidaan saada suhteellisen tarkkoja tuloksia käyttäen ASSET Radio:n järjestelmätason simulointia ja riippuen vaaditusta tarkkuustasosta, jättäen mahdollisesti mittaukset turhiksi.

Avainsanat: 5G NR, 5G mallinnus , 5G simulointi , 5G mittaukset

PREFACE

First of all, I would like to thank Oy Omnitele Ab for giving me an opportunity to do my master's thesis and allowing me to be a part of mobile network industry.

I would also like to express my deepest gratitude to team leader Päivi Haapala and senior consult Shahrukh Bin Ali for supporting me throughout the process and dedicating time to help me. I also wish to give acknowledgment to my colleague Marko Juvanen for always answering my inquiries.

Lastly, I would like to thank my supervisors Joonas Säe and Jukka Lempiäinen for giving me guidance and inspiration in this thesis work. Without their help, it would have not been possible for me to complete this thesis in time.

Tampere, 30th October 2022

Aki Pöyhönen

CONTENTS

LIST OF FIGURES

LIST OF TABLES

LIST OF SYMBOLS AND ABBREVIATIONS

1G	First generation
2G	Second generation
3G	Third generation
3GPP	3rd generation partnership project
4G	Fourth generation
5G	Fifth generation
5G-AN	5G access network
5GC	5G core network
$a(h_{\mathrm{M}})$	mobile station antenna height correction factor
AMF	Access and mobility management function
AMPS	Advanced mobile phone system
AR	Augmented reality
ARQ	Automatic repeat request
AS	Access stratum
BER	Bit error rate
BLER	Block error rate
C_M	constant offset in COST-231 Hata model
CDMA	Code-division multiple access
CNA	Cloud-native architecture
CP	Cyclic prefix
CRC	Cyclic redundancy check
d	distance
$\boldsymbol{\Delta f}$	subcarrier spacing
D-AMPS	Digital AMPS
d_0	reference distance
DAPS	Dual active protocol stack
DL	Downlink

DR	data rate
DRB	Data radio bearer
E-UTRAN	Evolved-UMTS terrestrial radio access network
EHC	Ethernet header compression
eMBB	Enhanced mobile broadband
en-gNB	Secondary-gNB
eNB	Evolved node B
EPC	Evolved packet core
f	frequency
$f^{(j)}$	scaling factor
FR	Frequency ranges
FTP	File transfer protocol
γ	path loss exponent
gNB	Next generation node B
GO	Geometrical optic
GSM	Global system for mobile communications
HARQ	Hybrid automatic repeat request
h_{B}	base station antenna effective height
h_{b}	base station antenna height above the ground
H_{eff}	effective base station antenna height
h_{M}	mobile station antenna effective height
H_{ms}	height of the mobile station above ground
h_{r}	receiver antenna height
HSPA	High-speed packet access
HTTP	Hypertext Transfer Protocol
iBLER	Initial block error rate
IMT-2020	International Mobile Telecommunications- 2020
IoT	Internet of things
IP	Internet protocol
ITU	International Telecommunication Union
J	sum of carriers
k	index of the subcarrier in the frequency domain

k_1	intercept
k_2	slope
k_3	mobile antenna height factor
k_4	multiplying factor for H_{ms}
k_5	effective antenna height gain
k_6	multiplying factor for the H_{eff}
k_7	multiplying factor for diffraction loss
L	path loss
l	OFDM symbol position in time domain
λ	wavelength
LCS	Location services
LOS	Line on sight
LPP	LTE positioning protocol
LTE	Long term evolution
μ	numerology
MAC	Medium access control
MME	Mobility management entity
mMTC	Massive machine type communications
MNO	Mobile network operators
MTU	Maximum transmission unit
NAS	Non-access stratum
$N_{PRB}^{BW(j),\mu}$	RB allocation in bandwidth $BW\left(j\right)$ with numerology μ
NG-RAN	Next generation RAN
NLOS	Non-LOS
NMFS	Network multimedia file system
NMT	Nordic mobile telephone
NR	New radio
NSA	Non-stand alone
OFDM	Orthogonal frequency-division multiplexing
$OH^{(j)}$	overhead
p	antenna port
PDC	Personal digital cellular

PDCP	Packet data convergence protocol
PDSCH	Physical Downlink Shared Channel
PDU	Protocol data unit
PHY	Physical layer
PRB	Physical resource block
PUSCH	Physical Uplink Shared Channel
QAM	Quadrature Amplitude Modulation
QCI	QoS class identifier
$Q_m^{(j)}$	modulation order
QoS	Quality of service
RAN	Radio access network
RLC	Radio link control
R_{max}	code rate
RMS	Root mean square
ROHC	Robust header compression
RRC	Radio resource control
RSSI	Received signal strength indicator
S	correction for shadowing
S-GW	Serving gateway
SA	Stand alone
SBR	Shooting and bouncing ray
SCS	Subcarrier spacing
SDAP	Service data adaptation protocol
SDU	Service data unit
SIM	Subscriber identity module
SL-DRB	Side link data radio bearer
SMS	Short message service
SN	Secondary node
SOR	Steering of roaming
SS-RSRP	Synchronization signal reference signal received power
SS-RSRQ	Synchronization signal reference signal received quality
SS-SINR	Synchronization signal signal-to-noise and interference ratio

SSB	Synchronisation signal block
SU-MIMO	Single-user multiple-input and multiple-output
SUI	Stanford university interim
TACS	Total access communications system
TB	Transport block
TCP	Transmission control protocol
TDD	Time division duplex
T_s^μ	average OFDM symbol duration in a subframe for numerology μ
UE	User equipment
UL	Uplink
UMTS	Universal mobile telecommunications system
UPF	User plane function
URLLC	Ultra-reliable low-latency communications
UTD	Uniform theory of diffraction
$v_{\text{Layers}}^{(j)}$	number of layers
VR	Virtual reality
WCDMA	Wideband code-division multiple access
X_{f}	correction for frequency
X_{h}	correction for receiving the antenna height

1. INTRODUCTION

This thesis aims to accurately simulate the 5G network using the radio network planning tool ASSET Radio and verify those simulated results with field measurement results. Ideally, the simulated result would match exactly to the field measurements results, but due to the multiple numbers of different variables which affect wireless networks, that is highly unlikely to happen. Analyzing the possible root causes, which leads to different results in simulation versus field measurements is also an important objective of this thesis.

The first part of the thesis is a 5G NR overview and propagation models, where the high-level description of 5G New Radio (NR) is provided and different types of propagation models are introduced. In the second part chosen important 5G User Equipment (UE) measurements in the scope of this thesis are made known along with the 5G Data Plane Stack to better understand throughput at different layers. In the third part, the 5G Radio Access Network (RAN) model and topology are represented along with an overview of the radio network planning tool ASSET Radio and simulation results. The fourth part focuses on the field measurements, which include an overview of the measurements, measurement equipment, techniques, and measurement results, along with a comparison to simulated results. The last part summarizes the results from the simulation and field measurements.

2. 5G NR OVERVIEW AND PROPAGATION MODELS

5G NR refers to the new radio access technology specification set by the 3rd Generation Partnership Project (3GPP) telecommunications standards group. It defines how 5G NR edge devices such as smartphones, routers, and gateways wirelessly transmit and receives data to/from 5G NR network infrastructure such as base stations and small cells by using radio waves.

5G networks will enable not only higher data rates but more reliable, low-latency communications and massive machine-to-machine communication, enabling new applications in many sectors. Furthermore, 5G networks are also expected to accelerate digitization and economic growth in a hyper-connected society, where not only people are connected to the network but devices and machines also.

The IMT-2020 (International Mobile Telecommunications- 2020) standards defined eight dimensions of enhancements to 5G network over 4G network [1]:

- Increased peak data rate
- Increased user-experienced data rate
- Increased spectrum efficiency
- Better support for mobility
- Decreased latency
- Increased area traffic capacity
- Increased connection density
- Increased network energy efficiency

Some of the 5G key features that enable these enhancements are introduced in section 2.3.

Propagation models are used to estimate accurate path loss in cellular network planning to optimize the cell tower distribution and predict coverage area and interference. These models are generalized to the specific environment depending on the area (urban, suburban, and rural), cell radius (macrocell, microcell, and picocell), and location (indoor or outdoor). Each model can be categorized into one of three types; empirical, semi-empirical, and deterministic. Empirical models are based on extensive measurements

and are widely used since they require only a few parameters to achieve acceptable prediction accuracy [2]. Semi-empirical models combine practically measured data and a few theoretical principles while deterministic models are purely based on Maxwell's equations, and they simulate the physical phenomenon of radio waves.

2.1 Evolution of mobile communications

The roots of mobile communications go as back as the 1980s when first-generation (1G) mobile systems set the first telecommunication standards for analog voice transmission, which were Nordic Mobile Telephone (NMT), Total Access Communications System (TACS), and Advanced Mobile Phone system (AMPS) [3]. The second generation (2G) was introduced in the late 1980s and it was based on digital transmission, which had several advantages over the 1G systems. 2G systems used Global System for Mobile Communications (GSM), digital AMPS (D-AMPS), code-division multiple access (CDMA), and personal digital cellular (PDC) standards. In the early 2000s, Universal Mobile Telecommunications System (UMTS) was introduced as third generation (3G) mobile cellular system. It used wideband code-division multiple access (WCDMA) and later high-speed packet access (HSPA) technologies to achieve better performance over previous systems [4]. Fourth generation (4G) mobile cellular system was introduced as Long Term Evolution (LTE) in 2008, which enabled global access, compatibility with other network technologies, and higher throughput [5]. The latest generation 5G was introduced in 2016 to meet the demands for higher speeds, lower latency, better reliability, and allowing a massive number of device connections. Figure 2.1 shows the evolution of mobile communications.

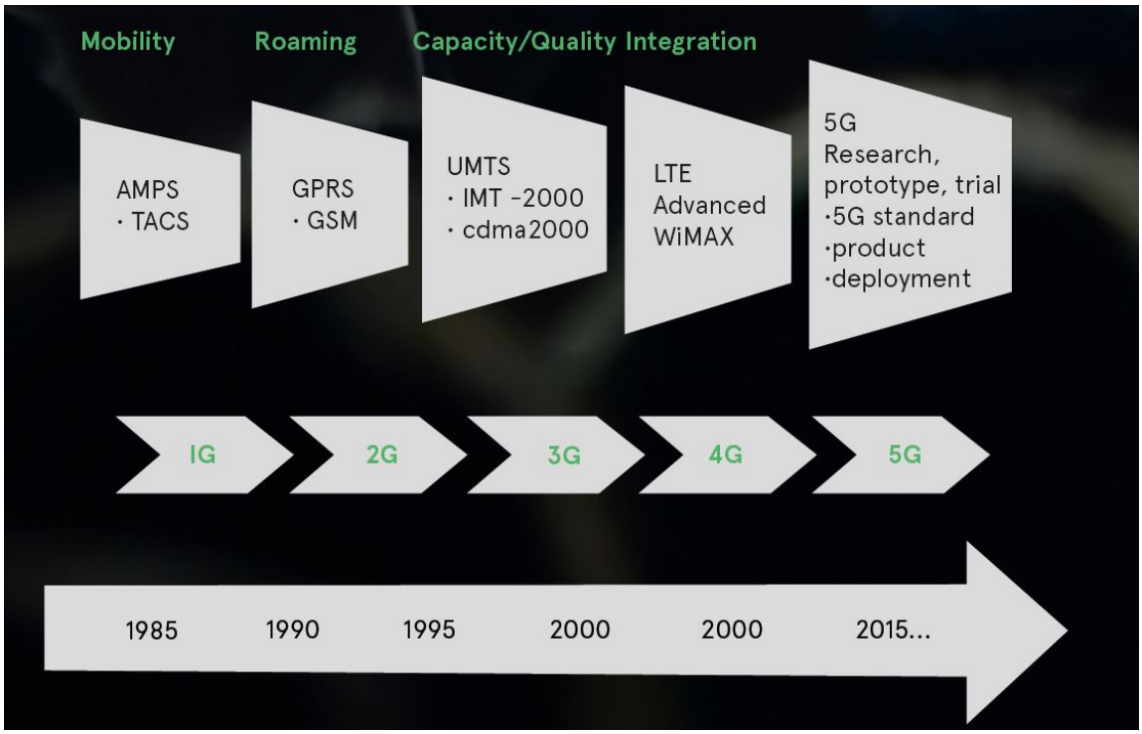

Figure 2.1. *Evolution of the mobile communications [6].*

2.2 5G use cases

Applications in 5G can be classified into three different use cases: massive machine type communications (mMTC), enhanced mobile broadband (eMBB), and ultra-reliable low-latency communications (URLLC). Figure 2.2 shows 5G use cases.

- Connectivity for a large number of devices, that transmits relatively low amounts of data is characterized as mMTC. These devices include use cases of the Internet of Things (IoT), which requires low power consumption and long battery life for applications such as smart factories, smart cities, and intelligent agriculture systems.
- Mobile users with better user experience than existing 4G networks are characterized as eMBB. It offers better capacity, enhanced connectivity, and better user mobility and will enable augmented reality (AR), virtual reality (VR), and 360° video streaming applications for example.
- Applications that are mission critical, which require exceptionally low latency, enormously high reliability, and good availability are characterized as URLLC. Example applications are remote surgery, autonomous vehicles, and tactile internet. [7]

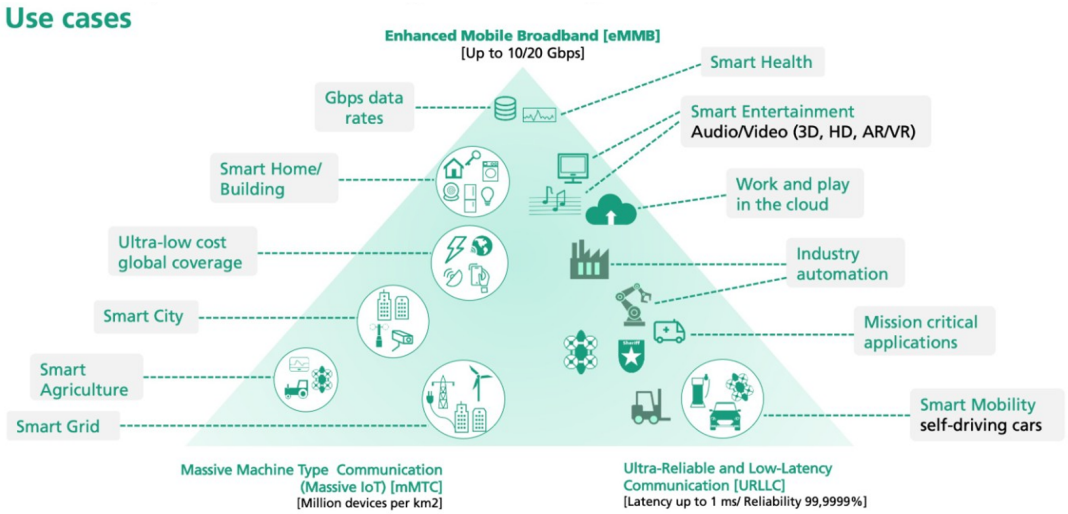

Figure 2.2. *5G Applications and Use Cases [1].*

2.3 5G features and architecture

The 5G network introduced various of different features compared to the 4G network to achieve better performance and to fulfill the 5G requirements set by the ITU (International Telecommunication Union) in IMT-2020 [1]. Key features of 5G are shown in Table 2.1.

Table 2.1. *5G key features [8].*

Feature	Benefit	Feature	Benefit
Usage of sub 6GHz and mmWave spectrum	10x...100x more capacity	**Advanced Channel Coding**	Large data block support with low complexity
UE agnostic Massive MIMO and beamforming	Higher Capacity and Coverage	**Aggregation of LTE + 5G Carriers**	Higher data rate with smooth migration
Lean carrier design	Low power consumption, less interference	**Integrated Access and Backhaul**	Greater coverage @ mmWave with lower cost
Flexible frame structure	Low latency, high efficiency	**Flexible connectivity, mobility and sessions**	Optimized end-to-end for any services
Scalable OFDM based air-interface	Address diverse spectrum and services	**Beamformed Control and Access Channels**	Greater Coverage
Scalable numerology	Support of multiple bandwidths and spectrum	**Higher Spectral Usage**	Enhanced Efficiency

The 5G System has three main components that 3GPP has defined: 5G Access Network (5G-AN), 5G Core Network (5GC), and UE. 5GC has the same idea of separating Control Plane functions from the User Plane as in 4G Core since it allows mobile network operators (MNO) to deploy and adapt the network as they see fit. [9]

3GPP defined two deployment options for 5G networks: Non-Stand Alone (NSA) Architecture and Stand-Alone (SA) architecture. NSA 5G utilizes the existing 4G network, while SA 5G is an independent system from the 4G network. In NSA 5G the 5G RAN is paired with the 4G Evolved Packet Core (EPC). This enables easier deployment and faster roll-out with reduced costs for 5G networks since MNOs can reuse their old infrastructure. The benefits of SA 5G are that it enables network slicing, virtualization, and cloud-native architecture (CNA) and MNOs can offer new 5G services such as smart factories, and smart cities [10],[11]. Figures 2.3 and 2.4 shows the NSA and SA architectures. Abbreviations in the Figures 2.3 and 2.4 stands for: Access and Mobility Management Function (AMF), User Plane Function (UPF), Next Generation Radio Access Network (NG-RAN), Next Generation Node B (gNB), Mobility Management Entity (MME), Serving Gateway (S-GW), Evolved Node B (eNB), Evolved-UMTS Terrestrial Radio Access Network (E-UTRAN) and Secondary-gNB (en-gNB).

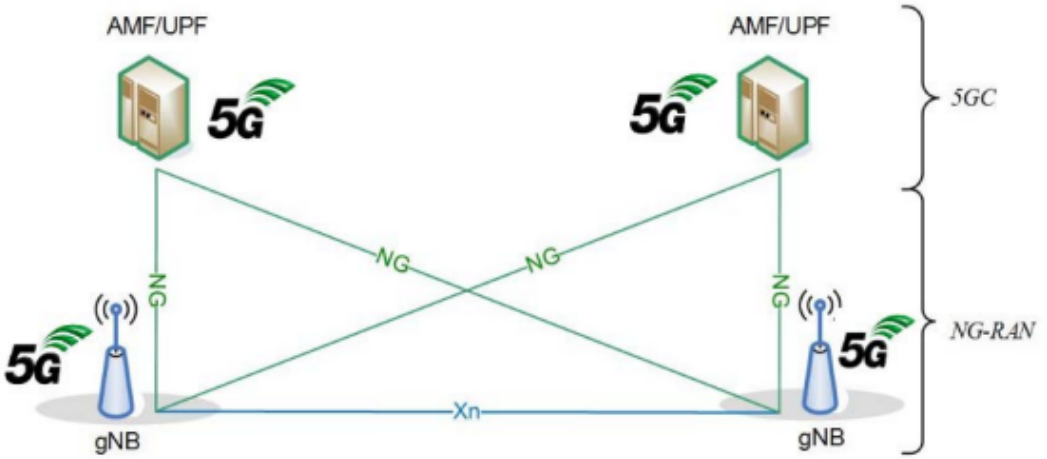

Figure 2.3. *The SA Architecture [11].*

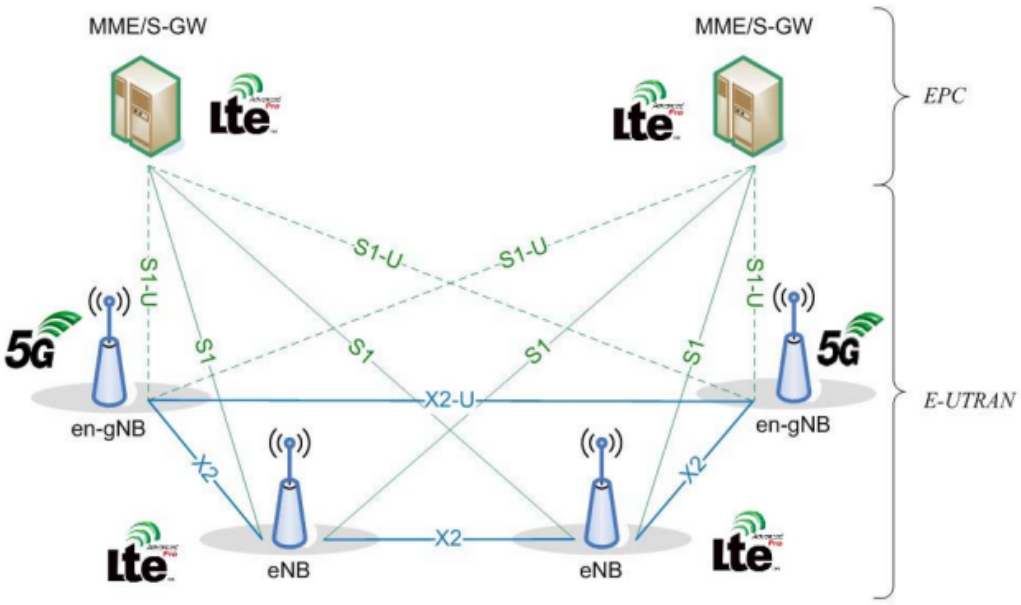

Figure 2.4. *The NSA Architecture [11].*

2.4 5G frame structure

5G NR has two frequency ranges (FR): FR1 for sub 6 GHz and FR2 for 24.25 GHz to 52.6 GHz [12]. Unlike in a 4G network, there are several different subcarrier spacing (SCS) Δf supported in 5G NR, which are described by numerology μ. In 5G NR each frame has a 10 ms duration and one frame consists of 10 subframes having a 1 ms duration each, and each subframe is divided into slots according to numerology. One slot has a fixed amount of Orthogonal frequency-division multiplexing (OFDM) symbols: 14 in case of normal cyclic prefix (CP) and 12 in case of extended CP. OFDM symbols in each slot are categorized as downlink, uplink or flexible (both downlink and uplink) transmission [13]. Table 2.2 shows transmission numerologies, which are supported in 5G NR. Table 2.3 shows numerologies related to OFDM symbols, slots, frames, and subframes for a normal cyclic prefix.

Table 2.2. *Supported transmission numerologies [14].*

μ	Δf [kHz]	**Cyclic prefix**
0	15	Normal
1	30	Normal
2	60	Normal,Extended
3	120	Normal
4	240	Normal

Table 2.3. *Number of slots in a sub-frame/frame for each numerology with normal cyclic prefix [14].*

μ	**No. of symbols per slot**	**No. of slots per subframe**	**No. of slots per radio frame**
0	14	1	10
1	14	2	20
2	14	4	40
3	14	8	80
4	14	16	160

Resources in 5G NR are mapped across a time and frequency grid, which is called a resource grid. It consists of several subcarriers in the frequency axis and several OFDM symbols in the time axis. The resource grid is made of resource elements, which are uniquely identified by $(k, l)_{p,\mu}$, where k is the index of the subcarrier in the frequency domain, l is the OFDM symbol position in the time domain, p is the antenna port and μ is the subcarrier spacing configuration. 12 consecutive subcarriers in the frequency domain form one Physical Resource block (PRB) and a single slot supports 24 to 275 PRBs [14]. Figure 2.5 shows the resource element, resource block, and resource grid in 5G NR.

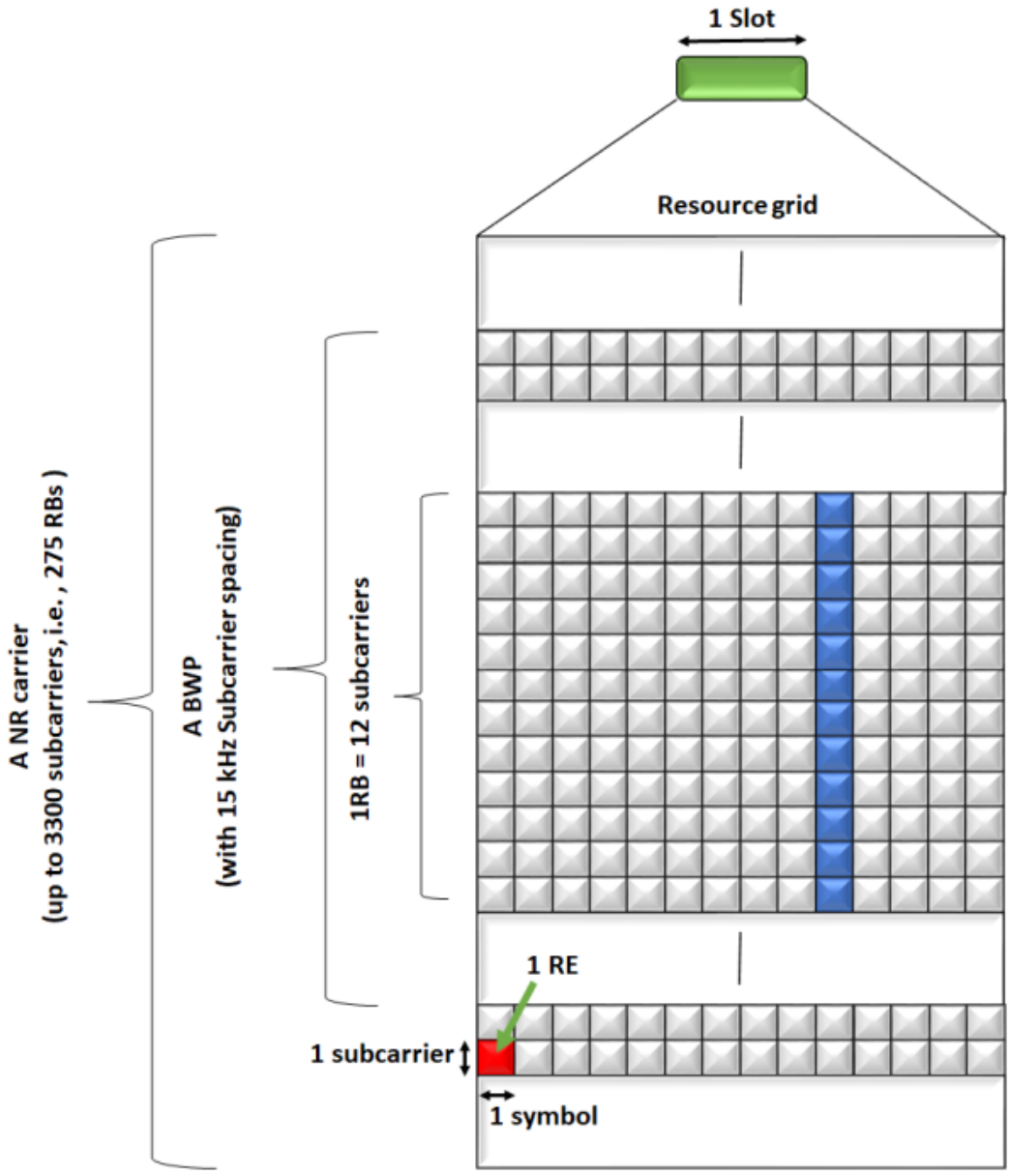

Figure 2.5. *Resource element, resource block, resource grid in 5G NR [15].*

2.5 Empirical models

The signal of wireless communication is affected by propagation factors such as free-space loss, absorption, scattering, diffraction, and reflection during transmission. Each of the empirical models is designed based on the measurements from specific environments, which gives a relatively good approximation of how propagation factors impact the signal in the measured environment. The advantage of empirical models is that they can be easily used in all kinds of environments, saving time and cost [16], [17]. In this section, three empirical models are introduced: Free Space Path Loss Model, the COST-231 Hata model, and Stanford University Interim (SUI) model.

Free Space Path Loss Model is the simplest path loss model to estimate signal strength since the model assumes that between transmitter and receiver is a clear line on sight (LOS) path. It is based on the Friis transmission formula and the generic expression for free space path loss is stated in equation 2.1. [18]

$$L = 32.45 + 20\log_{10}(d) + 20\log_{10}(f), \tag{2.1}$$

where L is the path loss in (dB), f is the frequency in (MHz) and d is the distance in (km).

COST-231 Hata model was deployed by European Cooperation in Science and Technology (COST) organization to extend the existing Hata model up to 2000 MHz. It was inspired by the increasing demand for GSM services, where the allocation of new channels was assigned to operate at the 1800 MHz frequency band. It is known that path loss can be much higher at the 1800–2000 MHz frequency band than in the 900 MHz range and studies have suggested that experienced path loss is roughly 10 dB bigger at 1845 MHz than at 955 MHz [19]. COST-231 Hata model covers the frequency range of 1500 MHz to 2000 MHz and shares the same other limitations as the Hata model. Limitations are listed below:

- Frequency Range f: 1500 MHz to 2000 MHz
- Base Station Antenna Effective Height h_{B}: 30 m to 200 m
- Mobile Station Antenna Effective Height h_{M}: 1 m to 10 m
- Link Distance d: 1 km to 20 km

COST-231 Hata model also contains correction factors for different types of the environment; urban, suburban, and rural. The path loss in COST-231 Hata model is calculated with equation 2.2 [20].

$$\begin{aligned} L = {} & 46.3 + 33.9\log_{10}(f) - 13.82\log_{10}(h_{\mathrm{B}}) \\ & - a(h_{\mathrm{M}}) + (44.9 - 6.55\log_{10}(h_{\mathrm{B}}))\log_{10}(d) + \mathrm{C_M}, \end{aligned} \tag{2.2}$$

where L is the path loss in (dB), f is the frequency in (MHz), d is the distance between transmitter and receiver in (km), and h_{B} is the base station antenna effective height above ground level in (m). The parameter $\mathrm{C_M}$ refers to constant offset and it is defined as 0 dB for medium-sized city and suburban centers with moderate city centers and 3 dB for metropolitan centers. The parameter $a(h_{\mathrm{M}})$ refers to mobile station antenna height correction factor and is defined for metropolitan centers in the equation 2.3 [21].

$$a(h_{\mathrm{M}}) = 3.2(\log_{10}(11.75h_{\mathrm{M}}))^2 - 4.97, \text{ for } f > 400 \text{ MHz} \tag{2.3}$$

and for the medium-sized city and suburban centers with moderate city centers in the

equation 2.4 [21]

$$a(h_{\mathsf{M}}) = (1.1\log_{10} f - 0.7)h_{\mathsf{M}} - (1.56\log_{10} f - 0.8), \tag{2.4}$$

where h_{M} is the mobile station antenna effective height in (m).

SUI model is an extension of the Hata model, and it allows the frequency band to extend up to 11 GHz. It was developed by Stanford University and it is suitable to use in the sites where receiver height is from 2 m to 10 m, the base station antenna height is from 10 m to 80 m, distance from the site is from 0.1 km to 8 km. There are three terrain types in the SUI model; Type A is suitable for hilly environments with moderate to heavy vegetation and presents the maximum path loss. Type B can be used for hilly terrains with rare vegetation, or flat terrains with moderate or heavy tree densities. Type C is recommended for flat terrain with light vegetation and presents the minimum path loss. The basic path loss formula for the SUI model is stated in equation 2.5.[2],[22]

$$L = A + 10\gamma\log\left(\frac{d}{d_0}\right) + X_{\mathsf{f}} + X_{\mathsf{h}} + S \quad \text{for} \quad d > d_0 \ , \tag{2.5}$$

where L is the path loss in (dB), γ is the path loss exponent, d is the distance from the base station to the mobile station in (m), d_0 = 100 m, X_{f} is the correction for frequency in (MHz), X_{h} is the correction for receiving the antenna height in (m) and S is the correction for shadowing in (dB) and its value is between 8.2 dB and 10.6 dB. The parameter A is calculated by equation 2.6. [2],[22]

$$A = 20\log(\frac{4\pi d_0}{\lambda}) \tag{2.6}$$

and the path loss exponent γ is calculated by equation 2.7 [2]

$$\gamma = \mathsf{a} - \mathsf{b}h_{\mathsf{b}} + (\frac{\mathsf{c}}{h_{\mathsf{b}}}), \tag{2.7}$$

where λ is the wavelength in (m) and h_{b} is the base station antenna height above the ground in (m) and its value is between 10 m and 80 m. The constants a, b and c are related to terrain types A, B and C, which are given in Table 2.4. Also, the value of path loss exponent $\gamma = 2$ for free space propagation, $3 < \gamma < 5$ for urban environment, and $\gamma > 5$ for indoor environment [22].

The correction factor X_{h} and correction for frequency X_{f} are calculated with equations 2.8,2.9 and 2.10 [2]:

$$\text{Terrain type A and B: } X_{\mathsf{h}} = -10.8\log(\frac{h_{\mathsf{r}}}{2000}) \ , \tag{2.8}$$

$$\text{Terrain type C: } X_{\text{h}} = -20\log(\frac{h_{\text{r}}}{2000}) \ , \tag{2.9}$$

$$X_{\text{f}} = 6\log(\frac{f}{2000}) \ . \tag{2.10}$$

Where h_{r} is the receiver antenna height in (m) and f is the frequency in (MHz).

Table 2.4. *Parameter values of SUI Model for different types of terrain.*

Parameter model	**Terrain A**	**Terrain B**	**Terrain C**
a	4.6000	4.0000	3.600
$b\ (m^{-1})$	0.00075	0.0065	0.005
$c\ (m)$	12.6000	17.1000	20.000

2.6 Other models

The semi-empirical model uses theoretical principles such as reflection, refraction, and diffraction along with practically measured data to achieve a more accurate model than a purely empirical model. Compared to the empirical model, the semi-empirical model also requires more computational time, since it needs more information about the propagation environment [23]. A deterministic model, on the other hand, is completely based on geometry and requires an extensive amount of geometrical information about the propagation environment, which makes the models most accurate but highly complex. In this section, one semi-empirical model and one deterministic model are introduced: Enhanced Macrocell Model and Ray tracing method.

Enhanced Macrocell Model is modified version of Standard Path Loss Model, which was developed based on the HATA model [24], [25]. Enhanced Macrocell Model is defined accordingly to the [26] as an “optimal dual slope loss model with respect to distance from the base station”. It takes into account the effects of clutter, diffraction loss, and effective base station heights. This model is suitable to use in the sites where receiver height is from 1 m to 10 m, the base station antenna height is from 15 m to 200 m, the distance from the site is greater than 500 m and the environment contains hilly terrain. The enhanced Macrocell Model also allows users to specify independent intercept and slope parameters for LOS and non-LOS (NLOS) environments. The path loss formula for Enhanced Macrocell Model is stated in equation 2.11.

$$\begin{aligned} L = {} & k_1 + k_2\log(d) + k_3\,(H_{\text{ms}}) + k_4\log\,(H_{\text{ms}}) \\ & + k_5\log\,(H_{\text{eff}}) + k_6\log\,(H_{\text{eff}})\,\log\,(d) + k_7\,(\text{diffn}) + \text{Clutter}. \end{aligned} \tag{2.11}$$

Where L is the path loss in (dB), d is the distance from the base station to the mobile station in (km), k_1 is the intercept, k_2 is the slope, k_3 is the mobile antenna height factor, H_{ms} is the height of the mobile station above ground in (m), k_4 is the multiplying factor for H_{ms}, k_5 is the effective antenna height gain, k_6 is the multiplying factor for $\log(H_{\text{eff}})\log(d)$, H_{eff} is the effective base station antenna height in (m), k_7 is the multiplying factor for diffraction loss calculation, diffn is the diffraction loss calculated by using either the Epstein-Peterson, Bullington, Deygout or Japanese Atlas knife edge techniques and Clutter is the clutter specifications taken into account in the calculation process. To clarify some factors: k_1 corresponds to a constant offset in (dB), k_2 to multiplying factor for the log of the distance between the transmitter and receiver, k_3 to the correction factor used to take into account the effective mobile antenna height and k_5 to multiplying factor for the log of the effective antenna height [26].

Ray tracing method utilizes Geometrical Optic (GO) and Uniform Theory of Diffraction (UTD) and provides accurate results both in indoor and outdoor urban environments. Ray tracing method solves numerically Maxwell's equations using ray-tracing algorithms, which are computationally complex. In the ray tracing method, Electromagnetic (EM) wave propagation can happen due to multiple mechanisms. Based on the behavior of one ray, four types of rays can be identified: direct rays, reflected rays, diffracted rays, and scattering. Ray-tracing algorithms try to determine the rays from a source location to a field point, taking into account all the ray types. There are four basic ray-tracing algorithms, which the ray tracing method can use: Fermat's principle of least time, image method, shooting and bouncing ray (SBR) method, and hybrid method. In Fermat's principle of least time, the ray travels from one point to another, which takes the least amount of time possible. The image method utilizes the trajectory of a reflected ray when the source point and the field point are known. The image method is best suitable for environments, where the number of reflection surfaces is minimal since computational time increases exponentially as the number of reflection surfaces increases. For a usual urban environment, the SBR method is more practical than the image method for predicting path loss. In SBR, all the rays that are launched from the source point are traced, to see if they reach the field point location. It is done in three steps: ray launching, ray tracing, and ray reception. The ray launching often requires uniform distribution of the rays from the source location, so each ray has similar power. In ray tracing idea is to determine whether the ray goes straight to the field point or does it hit an object and becomes reflected or diffracted. In the final step, the ray is tested for reception. As the ray travels, it is seen to be inside a ray tube and reception is tested by determining whether the field point is inside the ray tube or not. The hybrid method combines the image method and SBR method, by first using the SBR method to identify a valid ray and then using the image method to determine the trajectory of a reflected ray [27].

3. 5G UE MEASUREMENTS AND DATA PLANE STACK

In 5G NR, European Telecommunications Standards Institute (ETSI) has defined the UE measurement capabilities and in this section, the chosen UE measurements for this thesis are introduced. These are Synchronization Signal Reference Signal Received Power (SS-RSRP), Synchronization Signal Reference Signal Received Quality (SS-RSRQ), and Synchronization Signal signal-to-noise and interference ratio (SS-SINR) [28]. Also, the estimation for the 5G max data rate in the physical layer (PHY) is introduced.

SS-RSRP is defined according to the [28] as ”the linear average over the power contributions (in [W]) of the resource elements that carry secondary synchronization signals”. SS-RSPS are used for beam management procedures, cell selection, cell reselection, mobility procedures, and power control. Results are generated and reported at both layer 1 and layer 3.

SS-RSRQ is defined according to the [28] as ”the ratio of N$\times$SS-RSRP / NR carrier Received Signal Strength Indicator (RSSI), where N is the number of resource blocks in the NR carrier RSSI measurement bandwidth”. SS-RSPQ is used for cell selection, cell reselection, and mobility procedures.

SS-SINR is defined according to the [28] ”as the linear average over the power contribution (in [W]) of the resource elements carrying secondary synchronization signals divided by the linear average of the noise and interference power contribution (in [W])”. SS-SINR is used for mobility procedures in connected mode.

5G max data rate in PHY for uplink (UL) and downlink (DL) in (Mbit/s) is calculated with equation 3.1.

$$\text{Data rate} = 10^{-6} \cdot \sum_{j=1}^{J} (v_{\text{Layers}}^{(j)} \cdot Q_m^{(j)} \cdot f^{(j)} \cdot R_{\text{max}} \cdot \frac{N_{PRB}^{BW(j),\mu} \cdot 12}{T_s^{\mu}} \cdot (1 - OH^{(j)})), \tag{3.1}$$

where J is the sum of carriers, $v_{\text{Layers}}^{(j)}$ is the number of layers, $Q_m^{(j)}$ is the modulation order, $f^{(j)}$ is the scaling factor, R_{max} is the code rate, μ is the numerology, $N_{PRB}^{BW(j),\mu}$ is the RB allocation in bandwidth $BW\,(j)$ with numerology μ, T_s^{μ} is the average OFDM symbol duration in a subframe for numerology μ and $OH^{(j)}$ is the overhead. Scaling factor $f^{(j)}$ can have values 1, 0.8, 0.75 and 0.4. Overhead $OH^{(j)}$ can have the following

values: 0.14 for frequency range FR1 for DL, 0.18 for frequency range FR2 for DL, 0.08 for frequency range FR1 for UL and 0.10 for frequency range FR2 for UL [29].

Given the following parameters, which represent the simulated and measured environment, the 5G max data rate in PHY for DL can be estimated:

- J = 1
- $v_{\text{Layers}}^{(j)}$ = 4
- $Q_m^{(j)}$ = 8
- $f^{(j)}$ = 1
- R_{max} = 948/1024 = 0.92578125
- μ = 1
- $N_{PRB}^{BW(j),\mu}$ = 273
- $BW\,(j)$ = 100 MHz
- T_s^{μ} = $(10^{-}3)/(14 * 2^{\mu})$ = 0.00003571 s
- $OH^{(j)}$ = 0.14
- Parts of the slots allocated for DL = 4:1 = 0.8

$$\text{Data rate} = 10^{-6}\cdot 1\cdot 4\cdot 8\cdot 1\cdot 0.9258\cdot \frac{273\cdot 12}{0.000036}\cdot (1-0.14)\cdot 0.8, \tag{3.2}$$

which gives the data rate of 1870 Mbit/s. It is worth mentioning that this data rate for DL is highly theoretical since it assumes perfect radio channel conditions for maximum code rate along with modulation order of 8 and usage of 4 layers of Single-user Multiple-Input and Multiple-Output (SU-MIMO). Also, this DL data rate estimation is for the PHY throughput, while the end user will experience application layer throughput.

The protocol stack in 5G is highly similar to the 4G protocol stack because it also has two same categories: Control Plane Stack and User Plane Stack. Control Plane Stack is used for signaling or controlling messages, while User Plane Stack is used for user data. Both Control Plane Stack and User Plane Stack share the same structure for the first four layers: PHY, Medium access control (MAC), Radio Link Control (RLC), and Packet Data Convergence Protocol (PDCP) layers. After the PDCP layer, the User Plane Stack has Service Data Adaptation Protocol (SDAP) layer while Control Plane Stack has Radio Resource Control (RRC) and Non-access stratum (NAS) layers [30]. Figure 3.1 shows the 5G protocol stack. The main functions and services of each layer are introduced below.

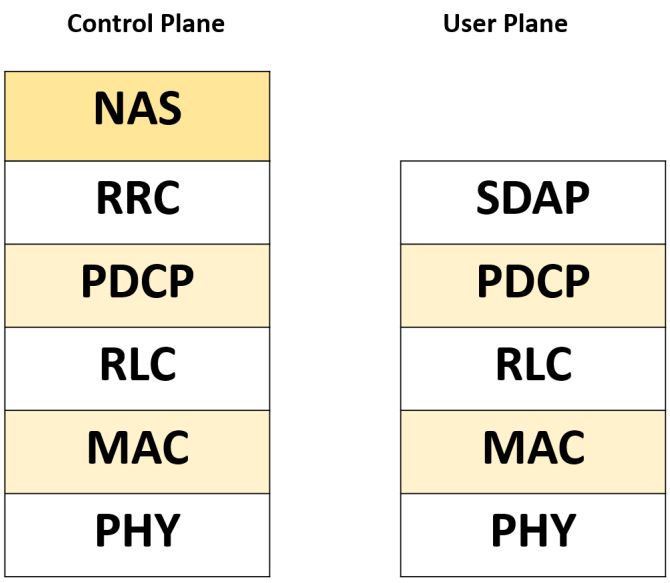

Figure 3.1. *5G protocol stack [30].*

MAC layer has the following functions [31]:

- mapping between logical channels and transport channels;
- multiplexing/demultiplexing of MAC service data units (SDU)s belonging to one or different logical channels into/from transport blocks (TB) delivered to/from the physical layer on transport channels;
- scheduling Information Reporting;
- error correction through Hybrid Automatic Repeat Request (HARQ);
- logical channel prioritization.

RLC layer has the following functions [32]:

- transfer of upper layer Protocol Data Units (PDU)s;
- sequence numbering independent of the one in PDCP;
- error correction through Automatic Repeat Request (ARQ);
- segmentation and re-segmentation;
- RLC SDU discard;
- reassembly of SDU;
- RLC re-establishment.

PDCP layer has the following functions and services [33]:

Services for the upper layers:

- transfer of user plane data;

- transfer of control plane data;
- header compression;
- ciphering;
- integrity protection.

Functions:

- maintenance of PDCP Secondary Nodes (SN)s;
- header compression and decompression using the Robust Header Compression (ROHC) protocol and Ethernet Header Compression (EHC) protocol;
- ciphering and deciphering;
- integrity protection and integrity verification;
- timer-based SDU discard;
- for split bearers and Dual Active Protocol Stack (DAPS) bearer, routing;
- duplication;
- reordering and in-order delivery;
- out-of-order delivery;
- duplicate discarding.

SDAP layer has the following functions [34]:

- transfer of user plane data;
- mapping between a Quality of Service (QoS) flow and a Data Radio Bearer (DRB) for both DL and UL;
- mapping between a PC5 QoS flow and a Side Link Data Radio Bearer (SL-DRB) for NR sidelink communication;
- marking QoS flow ID in both DL and UL packets;
- marking PC5 QoS flow ID in unicast of NR sidelink communication packets;
- reflective QoS flow to DRB mapping for the UL SDAP data PDUs.

RRC layer has the following functions [35]:

- establishment, maintenance, and release of an RRC connection between the UE and NG-RAN including addition, modification, and release of carrier aggregation;
- broadcast of System Information related to Access Stratum (AS) and NAS;
- paging initiated by 5GC or NG-RAN;

- mobility functions including Handover and context transfer; UE cell selection and reselection and control of cell selection and reselection; Inter-RAT mobility. QoS management functions;
- establishment, configuration, maintenance, and release of Signalling Radio Bearers (SRBs) and DRBs;
- security functions including key management;
- detection of and recovery from radio link failure;
- UE measurement reporting and control of the reporting;
- QoS management functions;
- NAS message transfer to/from NAS from/to UE.

NAS layer has the following functions [36]:

- support of mobility of the UE including also common procedures such as authentication, identification, generic UE configuration update, and security control mode procedures;
- support of session management procedures to establish and maintain data connectivity between the UE and the data network;
- NAS transport procedure to provide transport of Short Message Service (SMS), LTE Positioning Protocol (LPP), Location Services (LCS), UE policy container, Steering of Roaming (SOR) transparent container, and UE parameters update information payload.

From the User Plane perspective, each layer will reduce user throughput due to headers and there are still two layers after the SDAP layer; the Internet Protocol (IP) layer and lastly application layer. Throughput at the application layer is what the end user will experience and according to the study made by ETSI [37], user throughput at the application layer is approximately 5% smaller than in the PHY due to headers. Table 3.1 shows the 5G NR Data Plane Stack and header sizes for different layers. The Transmission Control Protocol (TCP) layer represents the application layer since for example File Transfer Protocol (FTP) runs on top of TCP and is commonly used by applications.

Table 3.1. *Header sizes for different layers in 5G[37].*

Protocol Layer	Header Size (Octet)
TCP	24
IP	24 for IPv4
SDAP	1
PDCP	7
RLC	5
MAC	3

For a typical transaction at the IP layer, the Maximum Transmission Unit (MTU) size is 1500 octets [37],[38]. Overhead between TCP and MAC layer can be calculated with the following equation 3.3:

$$OH = (\frac{1500 + 1 + 7 + 5 + 3}{1500 - 24 - 24}) - 1, \tag{3.3}$$

where OH is the overhead between TCP and MAC layer in (%). Equation 3.3 gives the overhead of 4.4%. Besides the overhead between the application layer and the MAC layer, user throughput is also affected by Initial Block Error Rate (iBLER) at the MAC layer and TCP packet loss at the application layer. The Block Error Rate (BLER) calculation is based on evaluating the cyclic redundancy check (CRC) on each Transport Block (TB). An erroneous block is a TB, of which the CRC is wrong. The first CRC Failure of TB CRC failure is considered as iBLER. The BLER target is maintained by the iBLER, which means that the network tries to maintain a predetermined iBLER value. This value is usually around 10% based on specifications but it can be varied depending on the characteristics of the cell.

In TCP, packet loss is usually caused by network congestion. This happens if network traffic hits its maximum capacity and data packets get backed up. This causes data packets to get lost, dropped, or not arrive in time. Generally speaking 1—2% packet loss is viewed as normal and acceptable, a higher packet loss value indicates that there are other network problems than congestion.

Overall, user throughput at the application layer is typically around 15—20% smaller than PHY throughput, due to headers, iBLER, and TCP packet loss.

4. 5G RAN SIMULATION

5G RAN simulation is done with the radio network planning tool ASSET Radio by TEOCO Corporation. The simulated area of the 5G RAN is a replica of the real-life 5G RAN by an anonymous commercial MNO. The purpose of the simulation is to get SS-RSRP, SS-RSRQ, SS-SINR, and data rates in the simulated area and later compare those results to field measurement results in that area. The simulated area is a typical suburban area and it only takes into account the 5G RAN, previous generation technologies are excluded from the simulation.

4.1 5G RAN model

The 5G RAN model in ASSET Radio includes clutter distribution/traffic spread, propagation model, antenna configuration, frame structure, terminal parameters, and 5G service parameters.

The clutter data is provided by a third party and it has a 25-meter resolution. There are six different types of clutter found in the simulated area: Forest, growth (0.5 m—5 m), apartment house area, small house area, business/industrial area, and urban area. Figure 4.1 shows the clutter distribution on the simulated area.

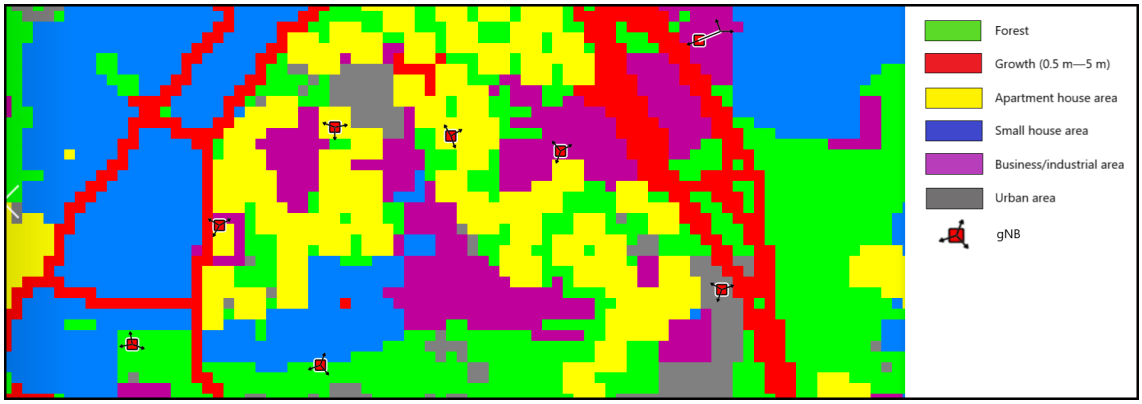

Figure 4.1. *Clutter distribution on the simulated area.*

Traffic is spread accordingly to each clutter type using predefined weights in clutter types. The predefined weights are used to spreading the traffic in a way, that resembles the real environment since it is highly more likely that the user is in the apartment house area than

in the forest for example. Table 4.1 shows the predefined weights in each clutter type that was used in the simulation.

Table 4.1. *Predefined clutter weights.*

Clutter type	**Weight**	**Normalized weight in%**
Forest	2	1.90
Growth (0.5m-5m)	2	1.90
Apartment house area	50	47.62
Small house area	25	23.81
Business/Industrial area	25	23.81
Urban area	2	1.90

In the simulation, both Non Busy-Hour and Busy-Hour scenarios were taken into account. In the Non Busy-Hour scenario, the simulated traffic amount was 66 simultaneous users and in the Busy-Hour scenario, the amount was 140 simultaneous users across all the cells. Traffic amounts were calculated by taking the average number of simultaneous users both in Non Busy-Hour and Busy-Hour time over 2 months using network data. Data showed that during a time window of 8 am to 9 pm, the lowest amount of simultaneous users was at 9 am and the highest amount was at 8 pm. The time window of 8 am to 9 pm was chosen to represent extended operating hours of business. Based on this data, Non Busy-Hour field measurements would start at 9 am and Busy-Hour field measurements at 8 pm.

Since the 5G field measurements are gonna be measured by driving a car in the actual location of the simulated area, the mobility of the simulated users needs to be the same. In each clutter type the minimum speed was set to 0 km/h, the mean speed to 20 km/h, and the maximum speed to 40 km/h, which represents relatively accurate speeds that the car experiences in the suburban environment.

Figure 4.2 shows the traffic spread in both scenarios along with a polygon area, that represents the area for the field measurements. The visualization of the traffic spread looks identical in both scenarios, but traffic density (terminals/square kilometer) is different.

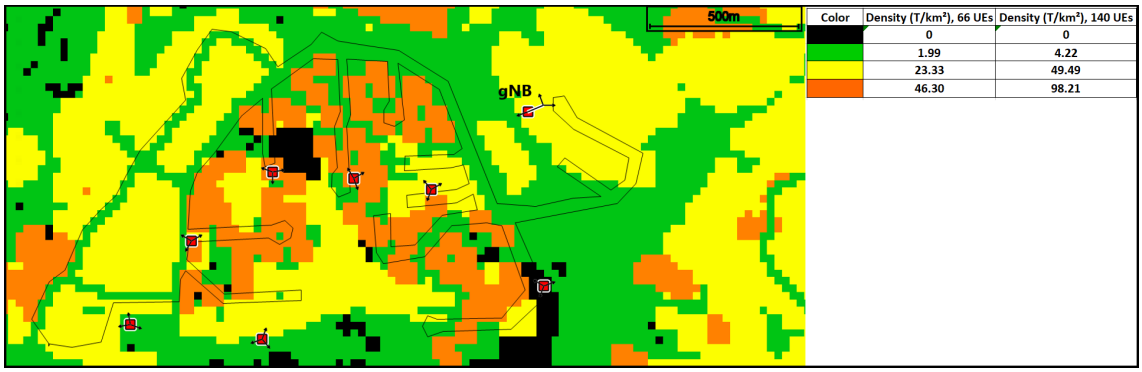

Figure 4.2. *Simulated traffic spread and field measurements area.*

ASSET Radio supports several propagation models for many different types of environments such as the Standard/Enhanced Macrocell model, Free Space Loss model, SUI model, and Volcano 3D ray-tracing model. In this simulation, Enhanced Macrocell Model was used, since it had been tuned to serve 3.5 GHz frequency in a suburban environment. Model tuning was done with ASSET Radio using its Automatic Model Tuning tool and the tuning was based on 5G field measurements in nine different areas. ASSET Radio Automatic Model Tuning tool objective is to minimize the Root Mean Square (RMS) of the error between the propagation model and the measurement data. In the tuned Enhanced Macrocell model the standard deviation of interference was 7.5 dB, mobile Rx height was 1.5 m and diffraction loss was calculated by using the Bullington method. Example of path loss calculation parameters and the clutter corrections are shown in the Tables 4.2 and 4.3.

Table 4.2. *Example path loss calculation parameters for 3.5 GHz frequency.*

LOS				**Common**	
k1:	167	k1 (near):	152.03	k3:	-3.20
k2:	44.9	k2 (near):	45.00	k4:	0.00
Use 'near' values when d <			0.2 km	k5:	-13.82
NLOS				k6:	-6.55
k1:	167	k1 (near):	156	k7:	0.80
k2:	44.9	k2 (near):	37.01		
Use 'near' values when d <			0.2 km		

Table 4.3. *Example clutter corrections for 3.5 GHz frequency.*

Clutter type	**Correction (dB/km)**
Forest	13.05
Growth (0.5m–5m)	-9.10
Apartment house area	20.05
Small house area	7.60
Business/Industrial area	4.85
Urban area	-0.04

The simulation used typical 5G beam-switching antennas with 8x8 MIMO (Multiple-Input and Multiple-Output) configuration. The antenna's transmit power was 53 dBm and it included 7 Synchronisation Signal Block (SSB) beam patterns and 127 traffic beam patterns. Figure 4.3 shows one of the SSB beam patterns and Figure 4.4 one of the traffic beam patterns, which were used in the simulation. Antennas transmission modes were set to 'Adaptive switching' both in downlink and uplink, meaning that they would choose either spatial multiplexing or spatial diversity, depending on the radio conditions. It is worth mentioning that the antennas used in the simulation are not the same antennas, that real-life 5G network use in the simulated area. However, since the exact number of SSB beams and traffic beams along with specific beam patterns are not public information, this antenna setup is the best estimate that can be used in the simulation.

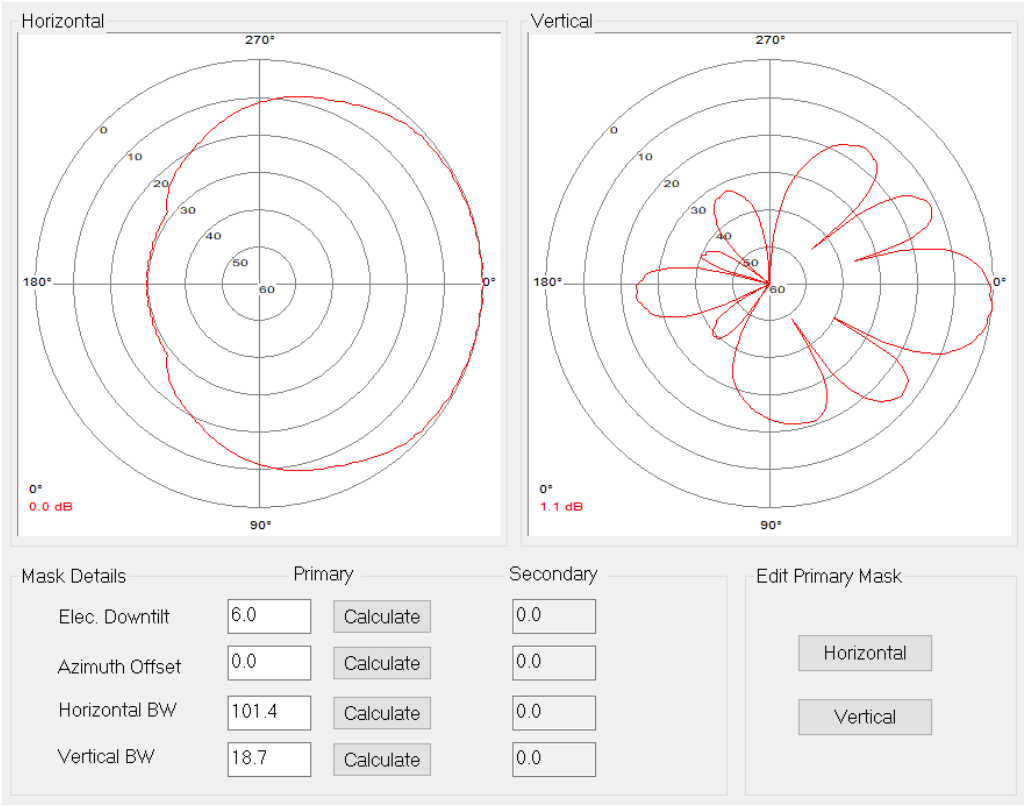

Figure 4.3. *Example of the SSB beam pattern [ASSET].*

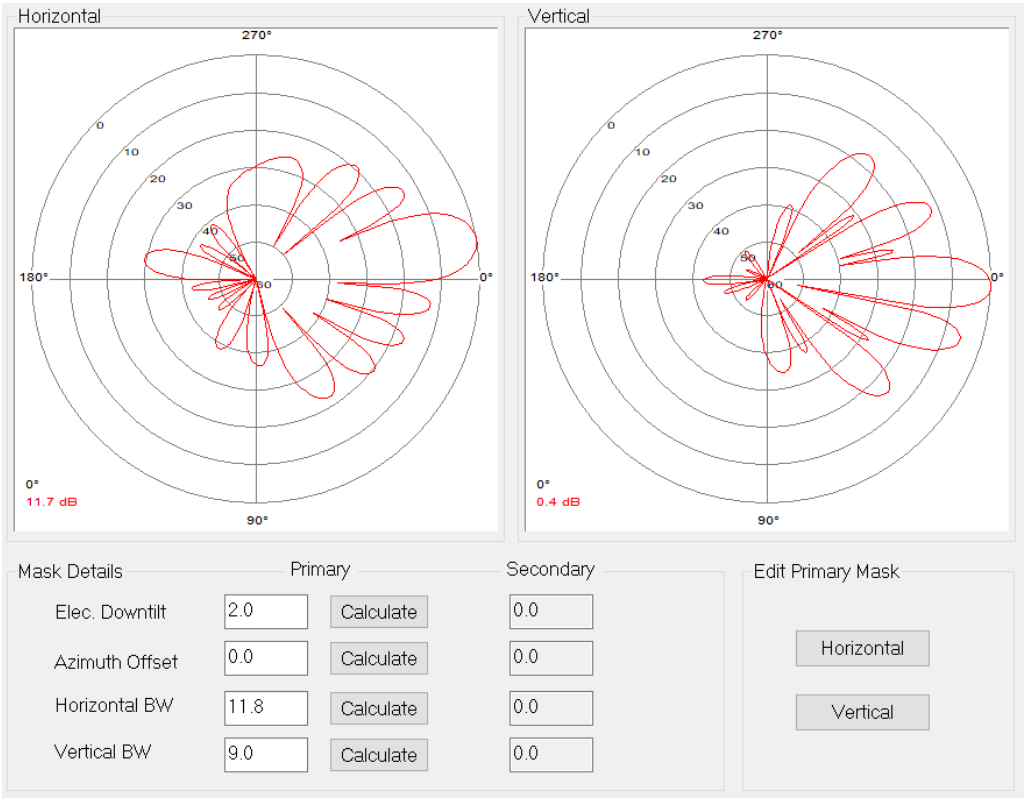

Figure 4.4. *Example of the traffic beam pattern [ASSET].*

The simulation was done with a 100 MHz time division duplex (TDD) carrier, which uses μ = 1 as numerology and a 4:1 ratio between downlink and uplink slots. Frame structure with SSB configuration is shown in Figure 4.5.

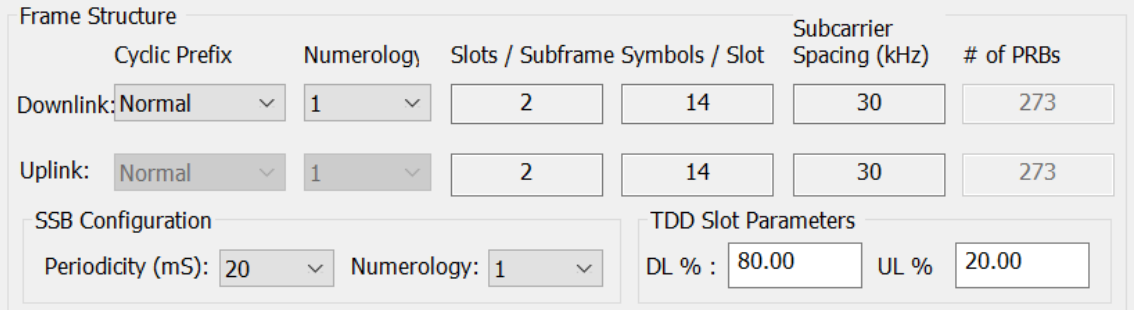

Figure 4.5. *Used frame structure [ASSET].*

In the field measurements, the OnePlus 9 phone was used as a terminal and the terminal parameters in the RAN model were configured to match the OnePlus 9 specifications. OnePlus 9 has 4 RX elements and 2 TX elements and the transmission mode is assumed to be 'Adaptive switching', since then the phone can utilize radio conditions the most efficiently. OnePlus 9 uses 256QAM (Quadrature Amplitude Modulation) in the downlink and 64QAM in the uplink. ASSET Radio also has a maximum service rate of 1 Gbit/s for each user, which represents a subscriber identity module (SIM) card subscription. The service rate was set to the maximum since in the field measurements SIM card with a 1 Gbit/s subscription is used. Terminal parameters that was used in the simulation are shown in the Figures 4.6 and 4.7.

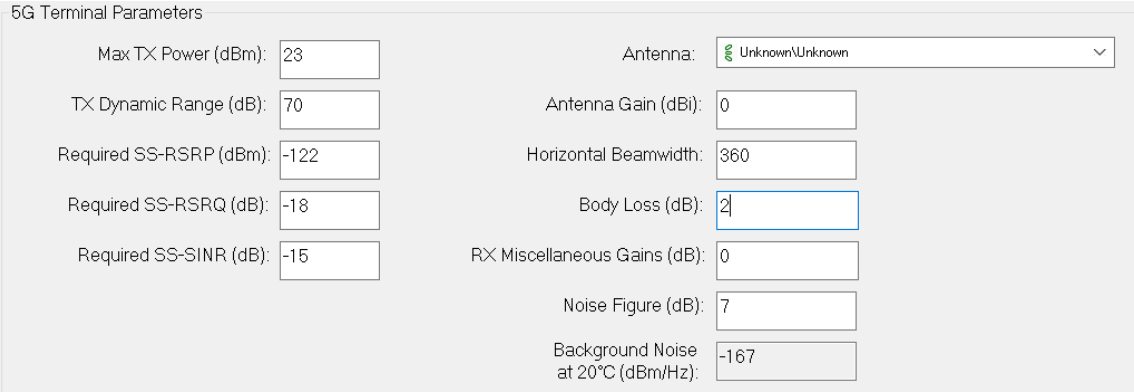

Figure 4.6. *Terminal parameters [ASSET].*

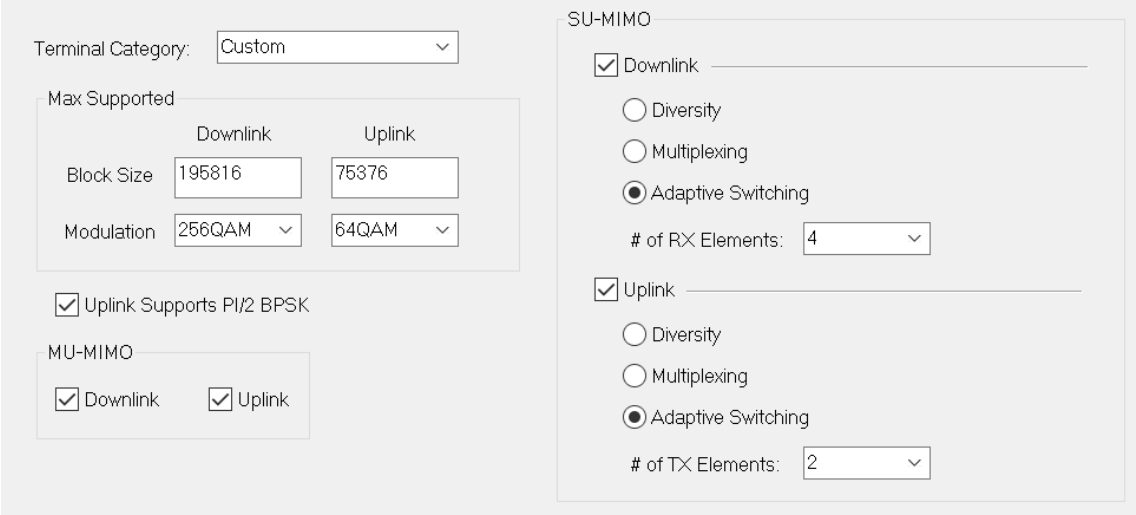

Figure 4.7. *Terminal parameters [ASSET].*

5G service parameters are shown in Figure 4.8. Traffic type was chosen as Real Time and traffic class as Non-Conversational Video since those represent the average user most accurately. The QoS class identifier (QCI) value in ASSET indicates priority to different services and since only one service is used in the simulation, the QCI value does not have an impact on the results.

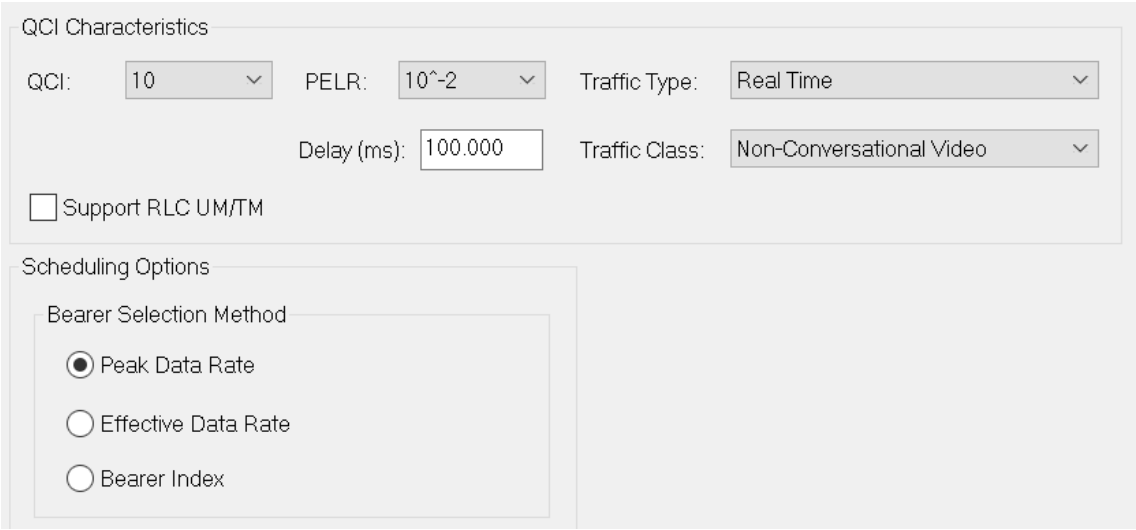

Figure 4.8. *5G service parameters [ASSET].*

4.2 5G RAN topology

The simulated area contains eight 5G base stations (gNBs) and each base station has three antennas, making a total of twenty-four 5G cells. Six base stations are located on the rooftops of apartment houses, one is located on the rooftop of an industrial building and one is located on the rooftop of a vocational school. Antenna heights vary from 16 meters to 33 meters and mechanical tilt was 5 degrees in all antennas. Electrical tilt

varied from 0 degrees to 13 degrees, depending on the used beam pattern. Geographical topology on the whole simulation area along with scale and polygon area representing field measurements area is shown in Figure 4.9. Antenna identities, heights, and azimuth angles are shown in Table 4.4.

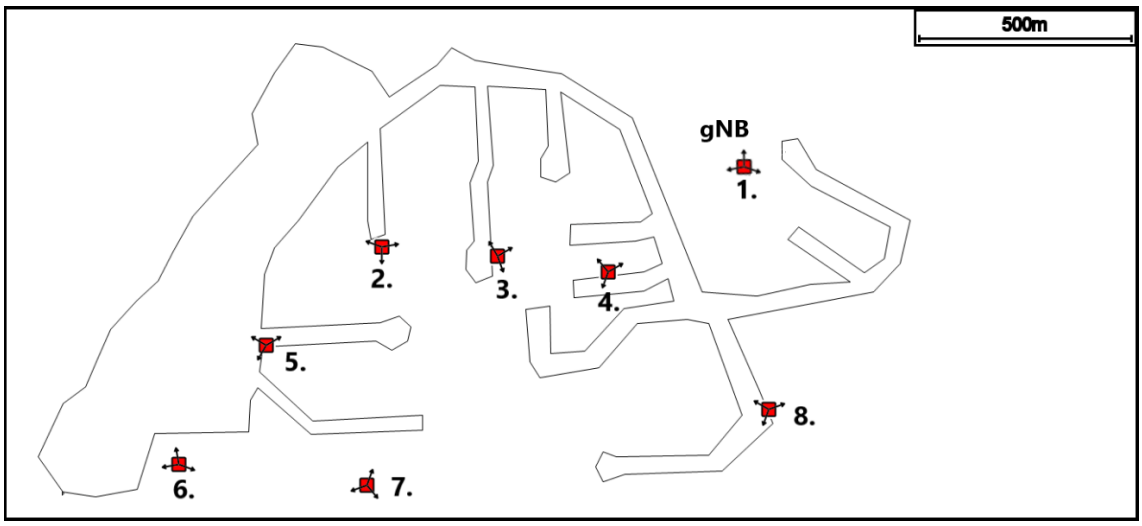

Figure 4.9. *Topology of the whole simulation area and field measurements area.*

Table 4.4. *Antenna identities, heights, and azimuth angles*

gNB - Antenna No. + (Identity)	Height (m)	Azimuth (°)
1-1 (1)	25	90
1-2 (2)	25	250
1-3 (3)	25	340
2-1 (4)	17	80
2-2 (5)	17	180
2-3 (6)	17	290
3-1 (7)	22	60
3-2 (8)	22	160
3-3 (9)	22	330
4-1 (10)	18	60
4-2 (11)	16	320
4-3 (12)	16	250
5-1 (13)	18	60
5-2 (14)	18	210
5-3 (15)	18	300
6-1 (16)	33	110
6-2 (17)	33	260
6-3 (18)	33	350
7-1 (19)	28	20
7-2 (20)	28	140
7-3 (21)	28	250
8-1 (22)	18	70
8-2 (23)	20	200
8-3 (24)	20	30

4.3 ASSET Radio overview

ASSET Radio provides capacity, RF coverage, cell parameter, and neighbor planning for cellular networks with the capability to run multiple technology simulations. It supports complex antenna arrays, 3D coverage, and advanced propagation models in 5G NR.

ASSET Radio can also be integrated with other ASSET products such as ASSET Capacity/Design/Geo to simulate end-to-end mobile networks and transmission layers, search for optimal network design and use geo-located traffic and performance maps.

4.3.1 Simulation principles

ASSET Radio simulation is based on static simulation, where the simulation model has no internal history of previous input or output values and does not have time as a factor. The static simulation model has a known function, which is made of inputs. Each simulation result is completely dependent on the function and input values. The performance of the network is analyzed from a series of randomized 'snapshots' of a system response on specific input values. Within each snapshot, the simulator calculates several performance metrics and results from a series of snapshots are then accumulated and averaged to form an estimate of the mean performance of the network. The problem with static simulation is accuracy since it does not take into account any different variations or scenarios that have an impact on the network such as the movement of the terminals. A more accurate simulation model would be a dynamic simulation since it has an internal memory of prior inputs, variables, and outputs. In a dynamic simulation, all the variables are denoted as functions of time, which makes it more accurate but also more complex.

In ASSET Radio the simulations are also described as system-level simulations, which provide important capacity and coverage metrics on the system/network level. On system-level simulation, multiple parameters regarding the simulated system are configured such as base stations, users, traffic model, antenna model, path loss model, and transmit power. Another simulation type is a link-level simulation, which focuses on point-to-point communication links and provides metrics such as bit/block error rate (BER)/(BLER) for a given signal-to-interference and noise ratio (SINR). In link-level simulation input parameters are related to the specific point-to-point communication link. Those parameters are such as channel coding, modulation, channel estimation, equalization, demodulation, and channel decoding.

4.3.2 Simulation steps

Before the network can be simulated in ASSET Radio, several steps need to be completed:

- Creating topology.
- Selecting/creating propagation model.
- Selecting/creating antenna.
- Configuring parameters.

- Creating traffic.
- Calculating path losses.

All of these steps are mentioned in previous sections, except calculating path losses.

Calculating path losses is done with 5G Coverage Wizard. In 5G Coverage Wizard four steps need to be completed before path losses can be calculated:

- Select area.
- Select sites.
- Select terminal type(s).
- Configure settings such as resolution and what carrier to use.

After the path loss calculation is completed, SS-RSRP values are visually shown on the map. Users can change visualization properties such as colors, ranges, min/max values, etc.

Now the network is ready to be simulated and it is done with 5G Simulator Wizard. In the 5G Simulator Wizard, the user configures simulation parameters such as selecting areas and sites, simulation resolution and enabling/disabling multipath arrays. After simulation parameters are set, Simulation Control Panel opens and simulation is done by hitting the 'run'. In Simulation Control Panel user chooses either to run a fixed number of snapshots or to run a 95 % confidence interval in dB, which refers to the confidence intervals for uplink noise rise and downlink traffic power on cells. Users can also run both choices or run one choice as many times as wanted since it will only increase the number of snapshots done. The simulation Control Panel is shown in Figure 4.10.

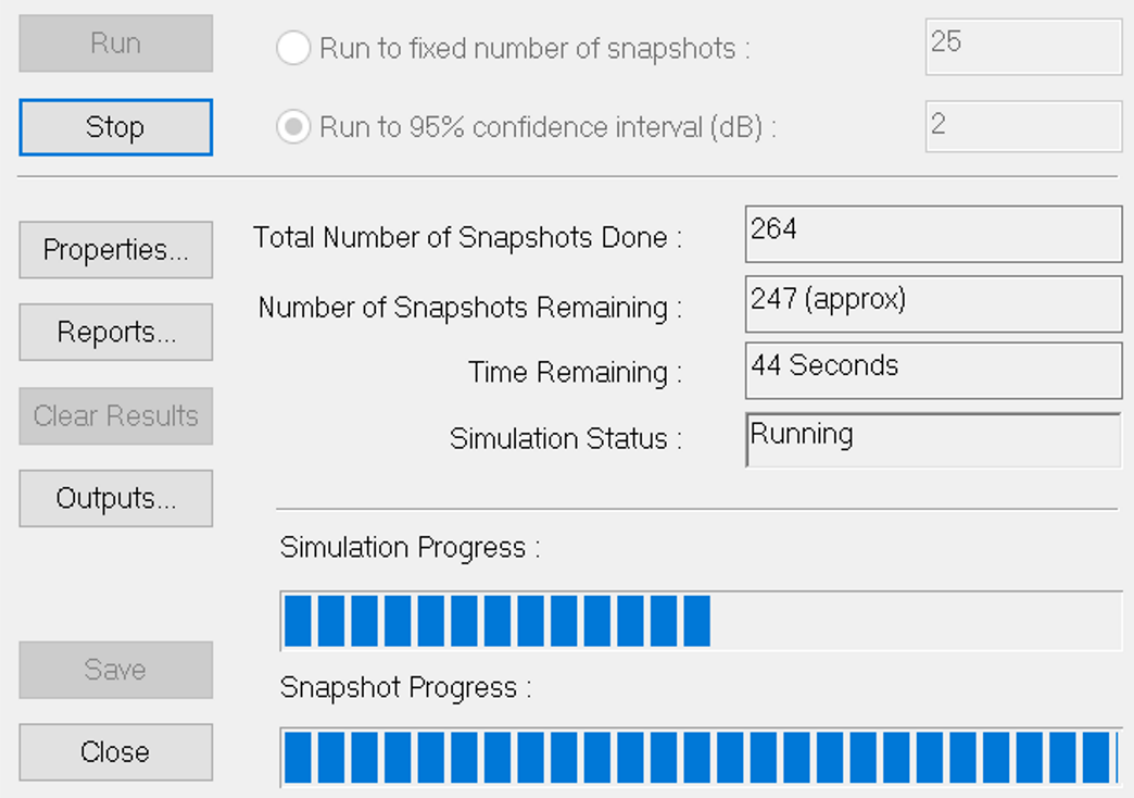

Figure 4.10. *Simulation Control Panel.*

4.4 Simulation results

The simulation was done with two different traffic scenarios, as mentioned before; the Non Busy-Hour scenario with 66 simultaneous users and the Busy-Hour scenario with 140 simultaneous users. The different traffic amount notably affects only the user throughput, while SS-RSRQ and SS-SINR stay nearly identical and SS-RSRP is not affected by traffic. In the SS-RSRQ and SS-SINR results only Non Busy-Hour scenario figures and statistics are shown since busy-hour scenario results were nearly identical.

Simulation results were taken after 1453 snapshots in the Non Busy-Hour scenario and after 1407 snapshots in the Busy-Hour scenario to ensure that the final results are as close to average as possible. The resolution in the simulation was 5 m, to achieve accurate results along with smooth figures.

4.4.1 Simulated SS-RSRP

Figure 4.11 shows the simulation results for SS-RSRP levels on the whole simulation area and Figure 4.12 shows the cumulative SS-RSRP on the polygon area. Cumulative SS-RSRP results are only taken from the polygon area since field measurements are going to take place only in that area. SS-RSRP levels in the heat map Figure 4.11 indicates that overall 5G coverage is excellent and statistics shown in Figure 4.12 confirms that 80%

of the polygon area had high (SS-RSRP level > -80 dBm) SS-RSRP levels. Given the fact that in terminal parameters the required SS-RSRP level was set to -122 dBm and the lowest level of SS-RSRP in the polygon area was -105 dBm, 5G coverage was 100%. It is worth mentioning that statistics show 5G coverage of 99.89%, which is the result of a few pixels being out of range on the high side, since the highest value that the heat map can show was set to -35 dBm.

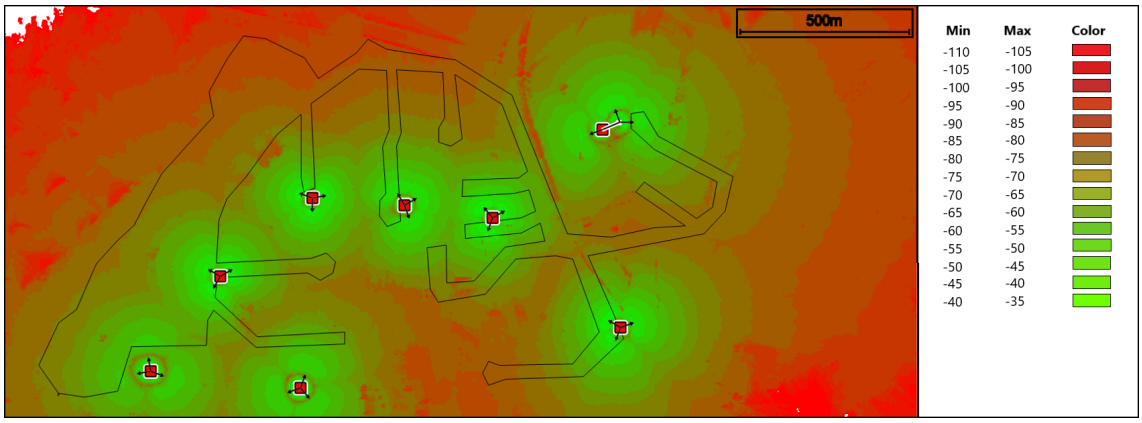

Figure 4.11. *Simulated SS-RSRP results on the whole area in (dBm).*

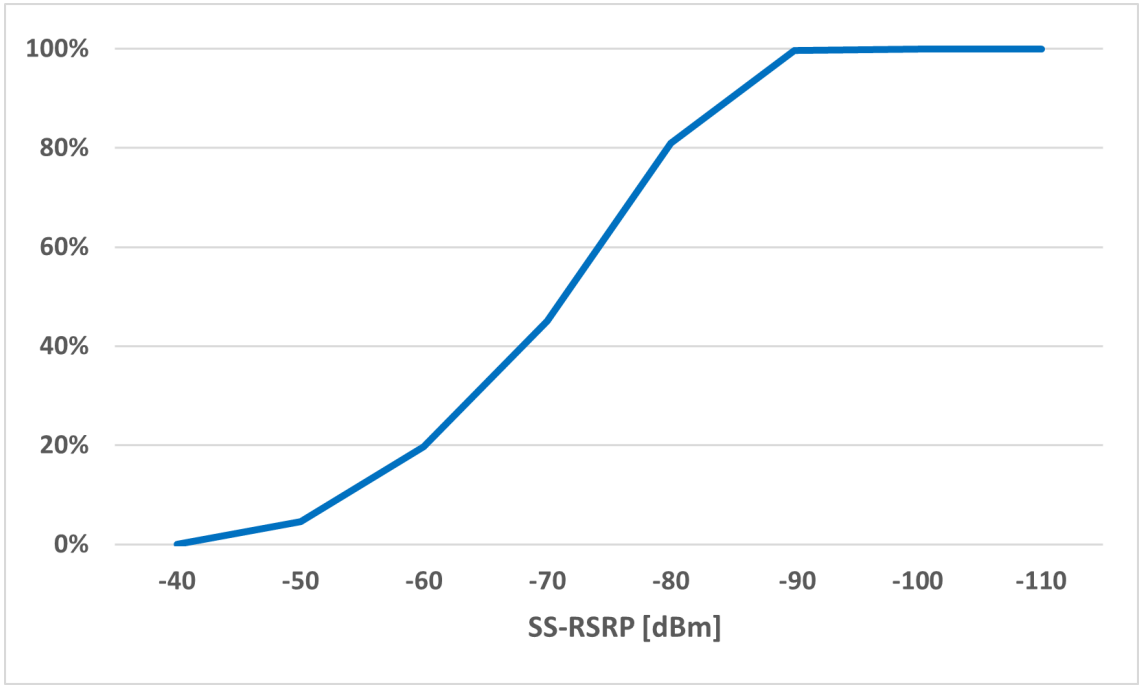

Figure 4.12. *Simulated cumulative SS-RSRP results on the polygon area.*

4.4.2 Simulated SS-RSRQ

SS-RSRQ levels in the heat map Figure 4.13 indicates that overall reference signal quality is decent in the simulated area, depending on what threshold of SS-RSRQ level is

considered to be good. Statistics show in Figure 4.14 that 80% of the polygon area had SS-RSRQ levels of -14 dB or higher. SS-RSRQ is essentially a signal-to-noise ratio measured using a standard signal since it is calculated by using SS-RSRP and RSSI, which includes interference and noise.

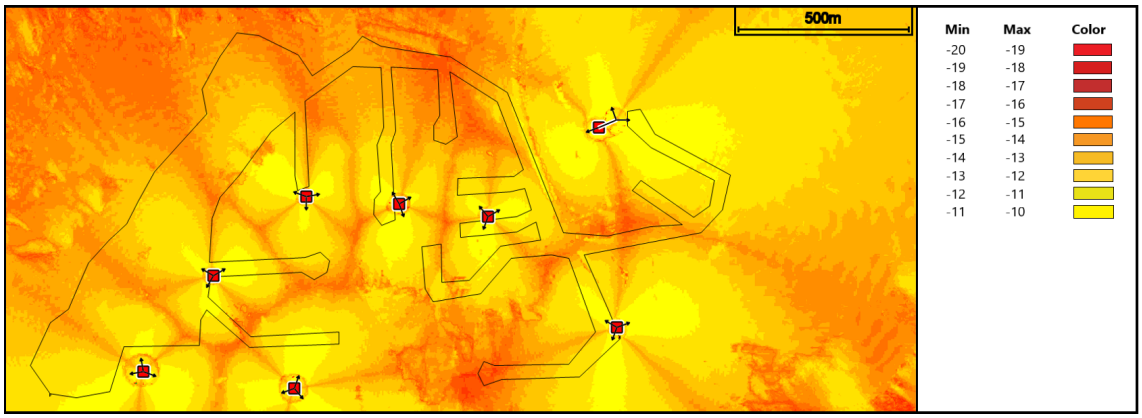

Figure 4.13. *Simulated SS-RSRQ results on the whole area in (dB).*

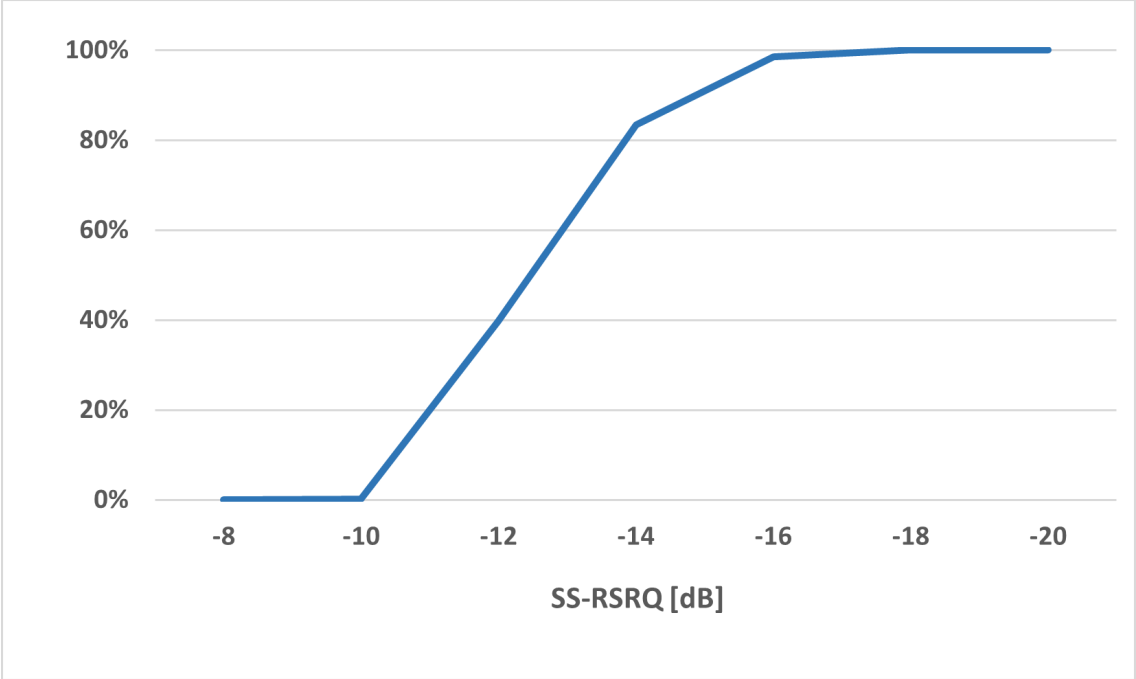

Figure 4.14. *Simulated cumulative SS-RSRQ results on the polygon area.*

4.4.3 Simulated SS-SINR

SS-SINR levels in the heat map Figure 4.15 indicates that overall signal quality is quite low in the simulated area. SS-SINR levels are only good in the proximity of antennas, which indicates that interference and noise quickly increase over signal strength as the distance to the antennas increases. Statistics show in Figure 4.16 that only 15% of the polygon area had good (SS-SINR level > 13 dB) SS-SINR levels. Probable causes for

low SS-SINR levels in the polygon area are high traffic amount, high density of cell sites, and ICI (inter-cell interference) at the edge of the cells.

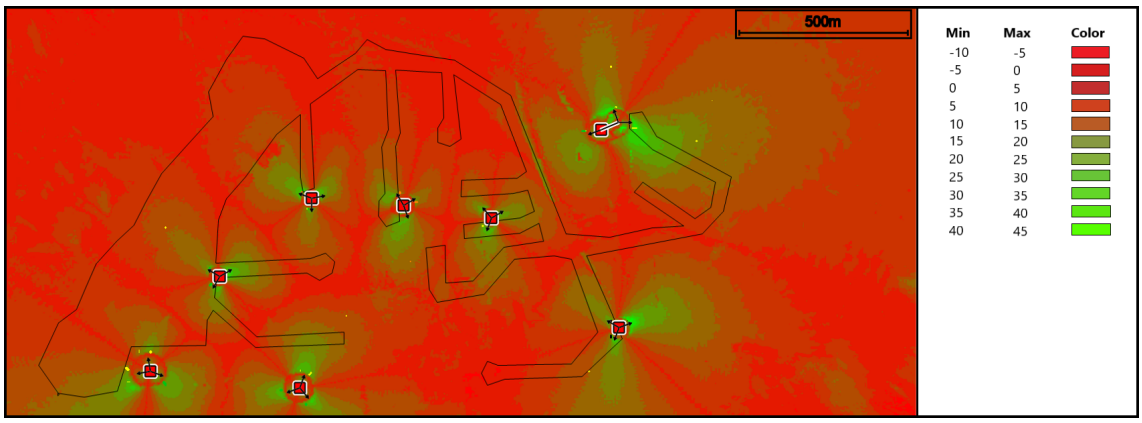

Figure 4.15. *Simulated SS-SINR results on the whole area in (dB).*

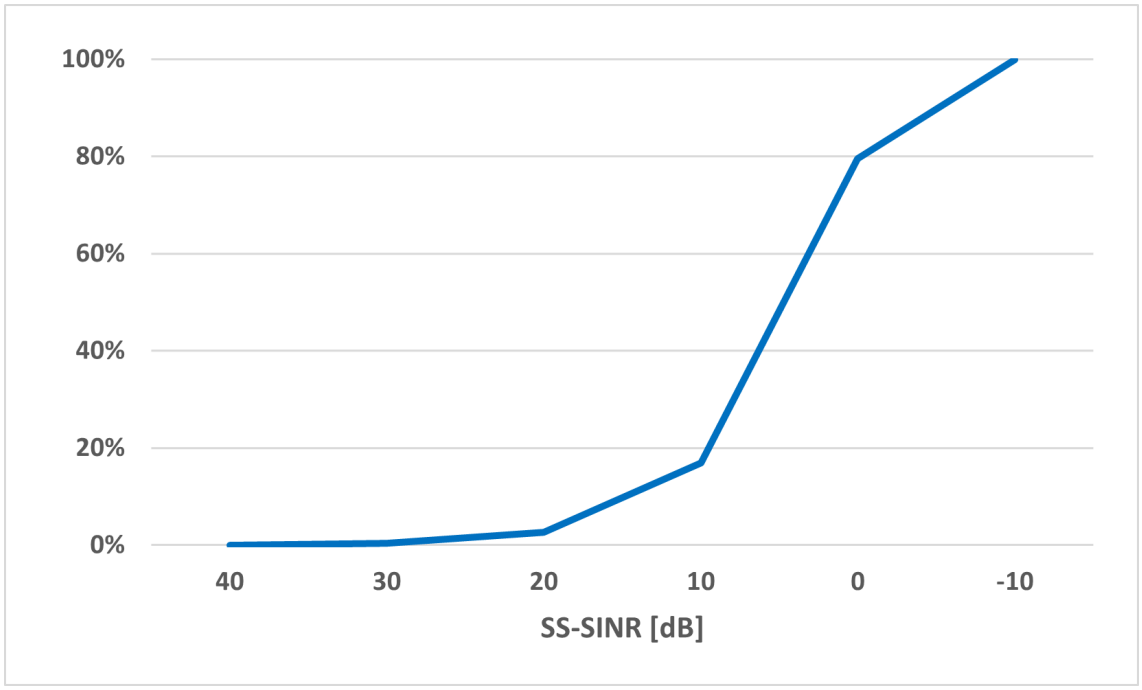

Figure 4.16. *Simulated cumulative SS-SINR results on the polygon area.*

4.4.4 Simulated user throughput

Average user application throughput was calculated by taking the total sum of served application throughput across all the cells and dividing it by the total number of served users. Figure 4.17 shows the simulated user throughput results in the downlink and uplink direction with both traffic scenarios.

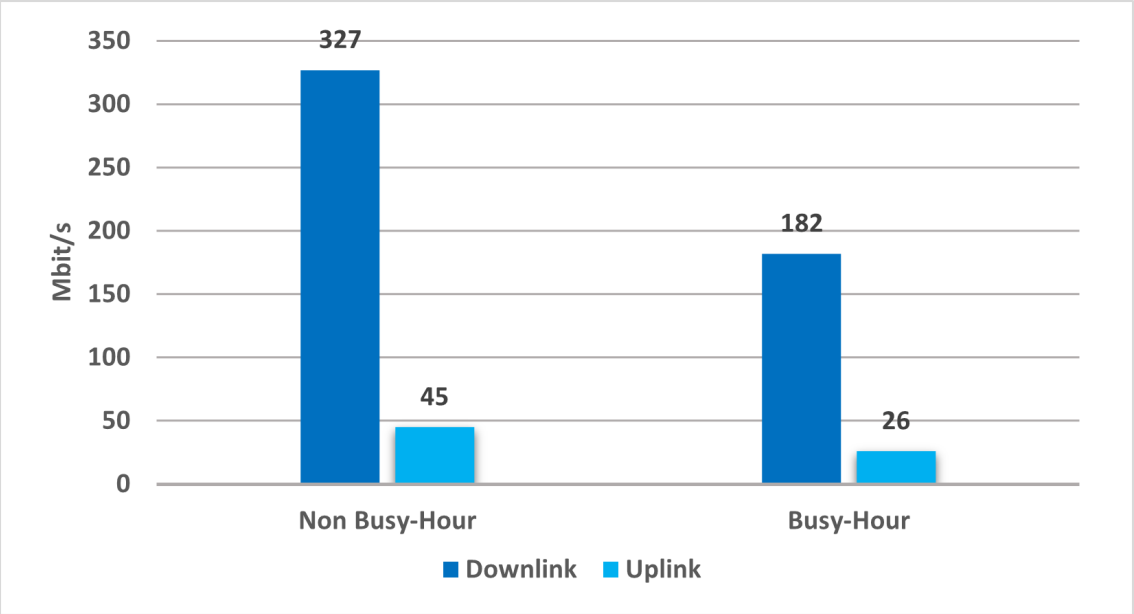

Figure 4.17. *Simulated user throughput in both traffic scenarios.*

Simulated downlink average user application throughput in the Non Busy-Hour scenario was 327 Mbit/s and 182 Mbit/s in the Busy-Hour scenario. Non Busy-Hour scenario provided almost double throughput compared to the Busy-Hour scenario, which seems plausible since the number of served users was also approximately double in the Busy-Hour scenario. Average cell utilization in the downlink direction in the Non Busy-Hour scenario was 68% and 84% in the Busy-Hour scenario. This indicates that even with the Non Busy-Hour scenario the cell's downlink capacity is almost already used and as the number of users increases, downlink user throughput is bound to drop.

Simulated uplink average user application throughput in the Non Busy-Hour scenario was 45 Mbit/s and 26 Mbit/s in the Busy-Hour scenario. Similar to downlink throughput, the ratio between Non Busy-Hour uplink throughput and Busy-Hour uplink throughput is approximately the same. Average cell utilization in uplink was 69% in the Non Busy-Hour scenario and 87% in the Busy-Hour scenario. This corresponds well with our previous interpretation that the cell's uplink capacity is almost already used in Non Busy-Hour scenario, which causes uplink user throughput to drop as the number of users increases. It is worth noting that there was a 4:1 ratio between downlink and uplink slots, and the ratio between downlink user throughput and uplink user throughput was close to 7:1. Probable causes for this is that UE's transmit power was 23 dBm and supported 64QAM modulation, while gNB antennas transmit power was 53 dBm and supported 256QAM modulation. Low transmit power and lower modulation limits UE's ability to send as much data uplink as gNBs can send to downlink. Also, having only two independent data streams in the uplink direction due to two TX elements limits the UL throughput compared to DL throughput, since in the downlink direction there can be up to four independent data streams due to four RX elements.

5. 5G FIELD MEASUREMENTS

5G field measurements were done by driving all the available roads in the simulated area with a car and measuring chosen relevant data during that drive. The route length was approximately 14 km and it took around 45 minutes to drive it, which gives a car a mean speed of 19 km/h. This correlates well with the mobility speeds that were set in the 5G RAN model. The route was driven at two different times;

- First drive started at 9 am, which represents the Non Busy-Hour scenario.
- Second drive started at 8 pm, which represents the Busy-Hour scenario.

5G scanner measured SS-RSRP, SS-RSRQ, and SS-SINR while data rates were measured with two 5G phones. One 5G phone had a SIM card with a 1 Gbit/s data rate subscription and the other 5G phone had a SIM card with an unlimited data rate subscription. The purpose of the other phone which had an unlimited data rate subscription was to see if was there any difference in data rates between those two phones due to different data rate subscriptions. The simulated user throughput will be compared to the phone which had a 1 Gbit/s data rate subscription since ASSET Radio also had that same limitation in the RAN model.

5.1 Equipment, setup and measurements

5G field measurements were done with the following equipment;

- Laptop with Nemo Outdoor software.
- Rohde & Schwarz TSME6 5G scanner.
- 2x OnePlus 9 phones.
- Antenna operating at 3.5 GHz frequency band.
- GPS antenna.
- Programmable USB hub.
- Inverter.
- Cables.

Figure 5.1 shows the equipment used in the field measurements.

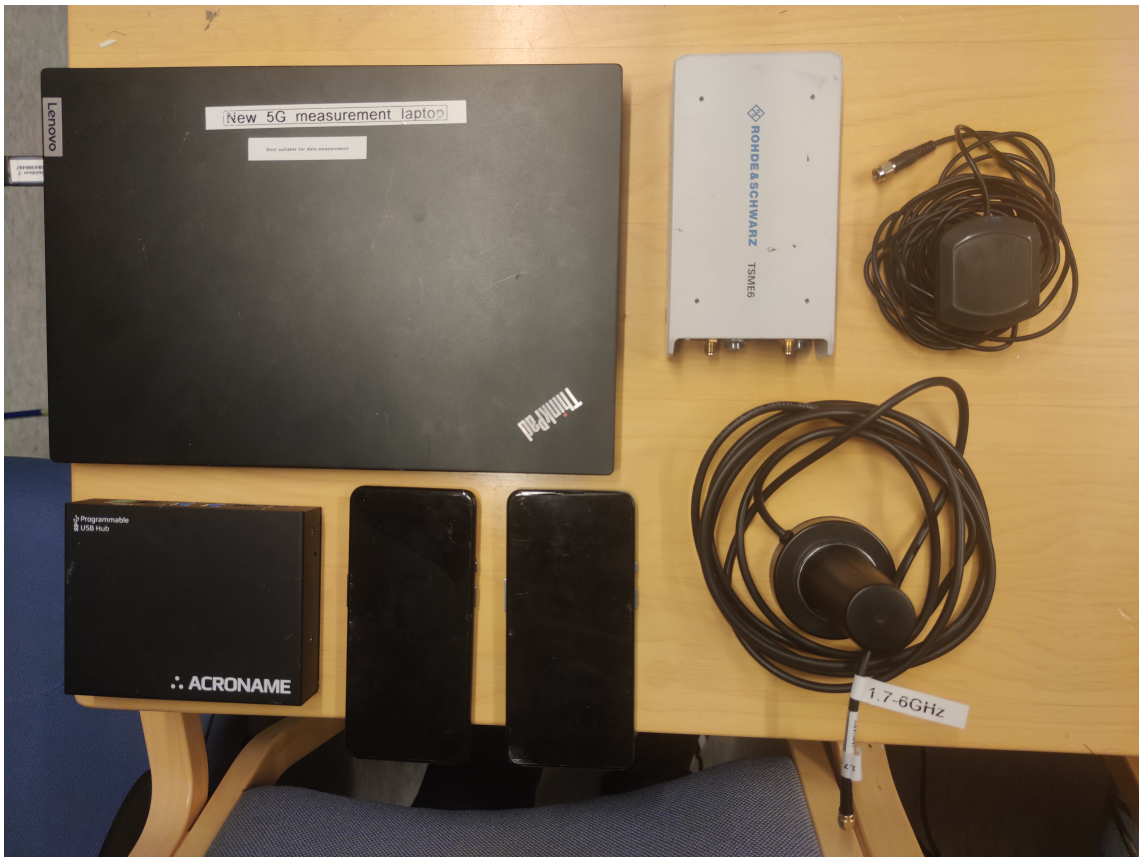

Figure 5.1. *Field measurement equipment.*

Nemo Outdoor is a laptop-based drive test tool for mobile network testing which supports over 300 devices and scanning receivers, from various vendors. It was used to collect all the relevant data from 5G scanner and 5G phones, which would later be analyzed with Nemo Analyze software. Nemo Outdoor functioned as a platform, where 5G scanner and 5G phones were connected during measurements. This enables a user to have full control of the measurement setup within one software.

Measurement setup were created by first connecting the 3.5 GHz antenna and GPS antenna along with the power cable to the TSME6 5G scanner. TSME6 5G scanner was then connected to the laptop with an Ethernet cable, where Nemo Outdoor auto-detects the scanner. After the scanner is detected, it needs to be configured what channels it will scan. In our case, the anonymous MNO had one 5G channel in the frequency band n78, which was selected. Two OnePlus 9 phones were connected to the programmable USB hub and that were connected to the laptop. Like with the scanner, Nemo Outdoor auto-detects OnePlus 9 phones and adds them to the hardware configuration. Phones, scanner, and laptop were powered by using an inverter that was connected to the car battery.

After the scanner and phones were connected to the Nemo Outdoor, a script needs to be made for the phones. When the measurements start, phones follow the predeter-

mined script, which controls how long phones download and upload data from desired servers and how long phones wait between download and upload. In our case, the script starts with a 5-second wait, then 60 seconds of download or upload from/to the Hypertext Transfer Protocol (HTTP) server depending on the phone, then 20 seconds wait, then 60 seconds of download or upload from/to HTTP server depending on the phone and lastly 15 seconds wait before the loop starts over. The phones had different scripts, where one phone starts the measurements by downloading data and the other one by uploading data. This enables phones to download and upload data in a way, that another phone has minimal impact on the other. The data is downloaded from two different servers simultaneously and uploaded to one server. This provides two different data rates whenever the phone is downloading and the measured DL data rate is a sum of those two data rates. The scanner is 'always on, so it does not require any script. Figure 5.2 shows the script used when measurements start with uploading the data.

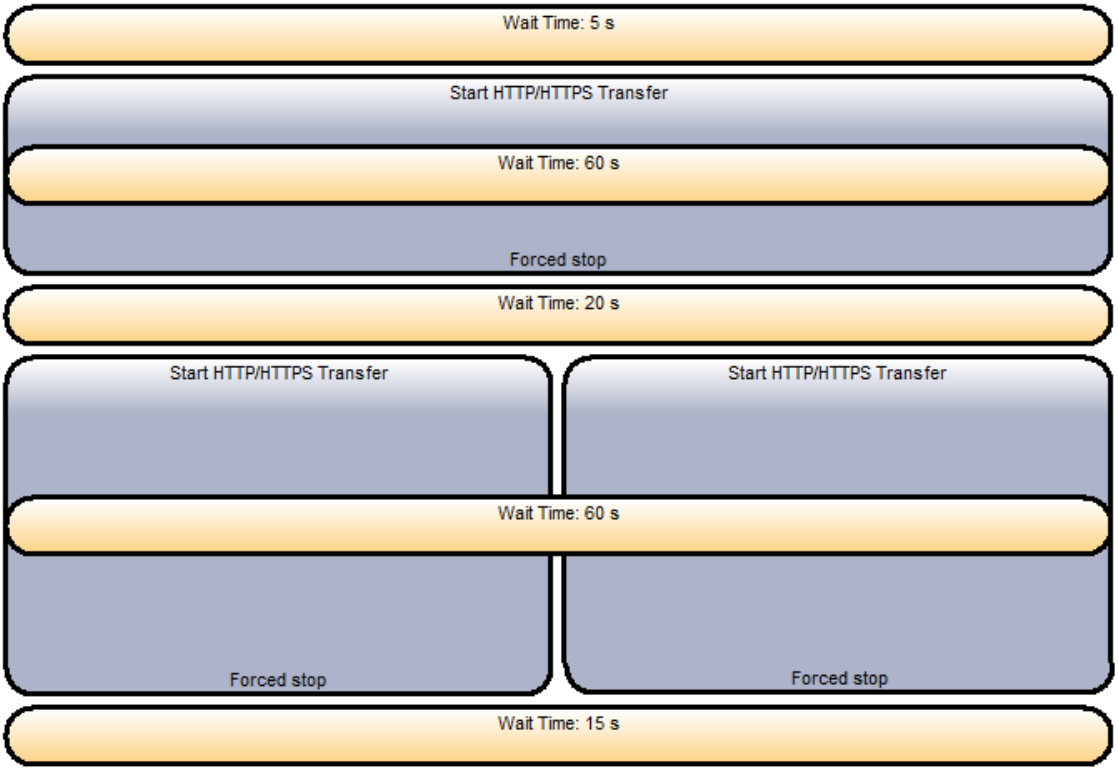

Figure 5.2. *Measurement script starting with the upload.*

After the scripts were made for both phones, a workspace needs to be created in the Nemo Outdoor to visually confirm that everything is functioning properly during the measurements. In the workspace, the user can create as many tabs as needed. In our case, four tabs were created. The first tab showed general information on the phones and the scanner such as GPS status, temperatures, and connected network. This enabled a user to see the overall status of the measurements and notice if something was wrong. For example, if the temperatures of the phones are high and they are connected to the 4G

network, it could indicate that the phone's temperatures are too high to connect to the 5G network and measurement results are not desired. The second tab was a map view, which showed your current location and driven route. This enabled a user to confirm that GPS was working properly and all the desired roads have been driven. The third tab showed application throughput on both phones in the downlink and uplink direction. Application throughput was shown visually in the line graphs and it enabled users to see current user application throughput on both phones. The fourth tab showed SS-RSRP, SS-RSRQ, and SS-SINR visually in the line graphs to confirm that scanner was measuring everything properly. This was also an important indicator that measurements were functioning the desired way since sometimes the scanner would lose connection to the Nemo Outdoor and require rebooting.

During the measurements, it was important to check the phone's temperature on the general information tab, since there have been problems where phones could not connect to the 5G network probably due to high temperature. This is pure speculation based on multiple measurement projects, where there has been a clear correlation between the high phone's temperature (T > 55 °C) and the inability to connect to the 5G network. If the speculation is correct, this is probably a phone's safety feature to prevent overheating. This problem was solved by turning the phones off for 10 minutes and placing them away from direct sunlight, so they can cool off. Also, during one measurement drive, there was a mass event taking place in the sports center near the measurement route. Those results needed to be removed, since they did not represent the normal measurement circumstances. Other tabs were displayed occasionally to ensure that GPS and scanner were working in the desired way. Figure 5.3 shows the outlook of the Nemo Outdoor software.

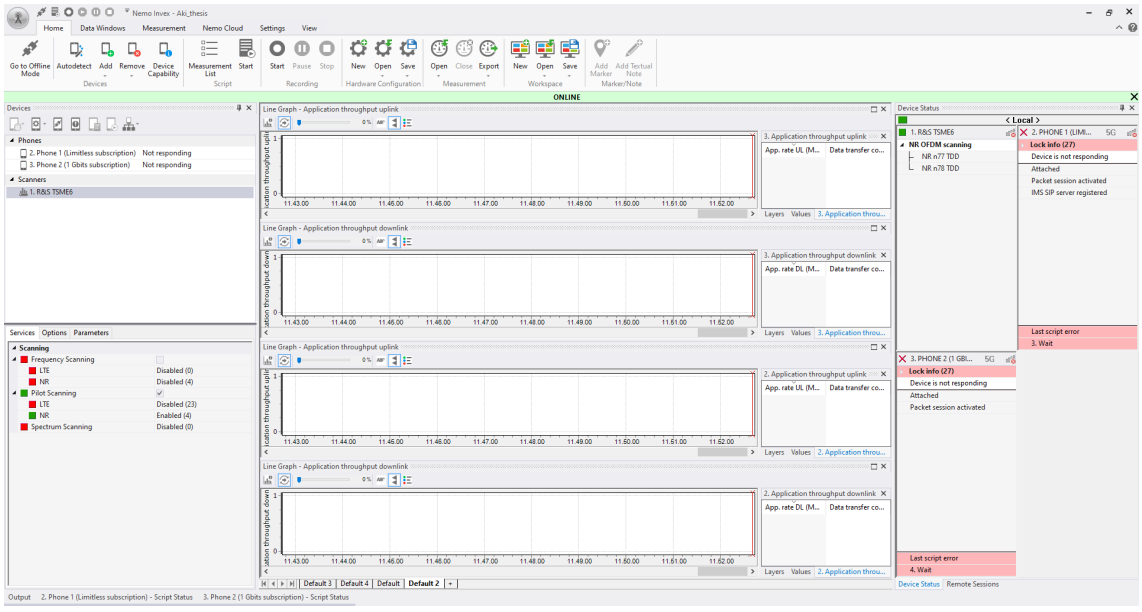

Figure 5.3. *Outlook of the Nemo Outdoor software.*

5.2 Measurement results

Nemo Outdoor saves the measurement results individually for each device and scanner in a file format called Network Multimedia File System (NMFS). Analyzing the measurement results requires Nemo Analyze software with a license. Nemo Analyze is a desktop-based tool for analyzing data from Nemo products and it has a comprehensive set of data visualization techniques.

5.2.1 Measured SS-RSRP

Measured SS-RSRP levels from the Busy-Hour scenario drive test are shown in Figure 5.4. The squares with black outlines in Figure 5.4 represent the locations of the gNBs in the measured area. Figure 5.5 shows the cumulative SS-RSRP on the simulated results and measured results on the same graph. Measurements results in the Non Busy-Hour scenario are not shown, since traffic amount does not affect SS-RSRP levels.

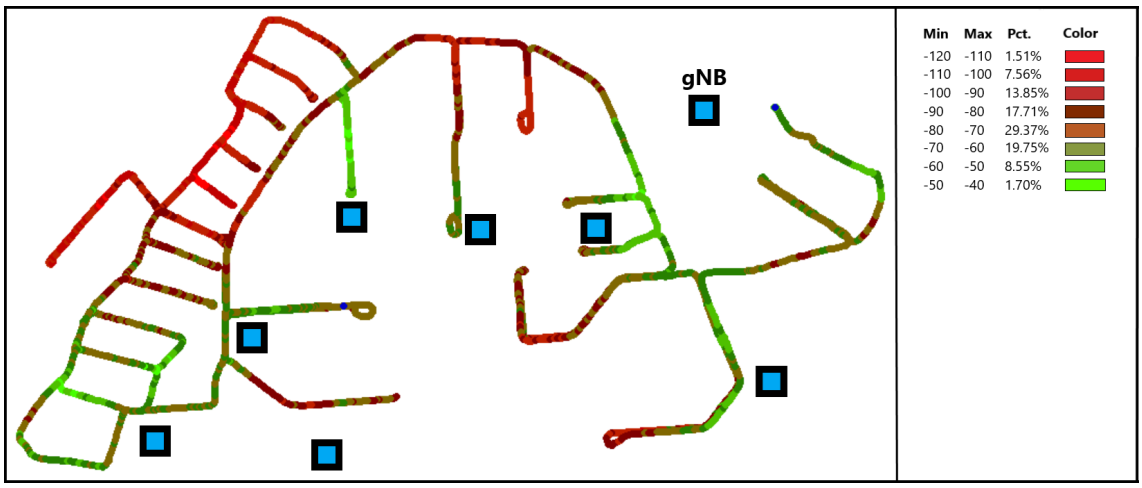

Figure 5.4. *SS-RSRP measurement results in (dBm).*

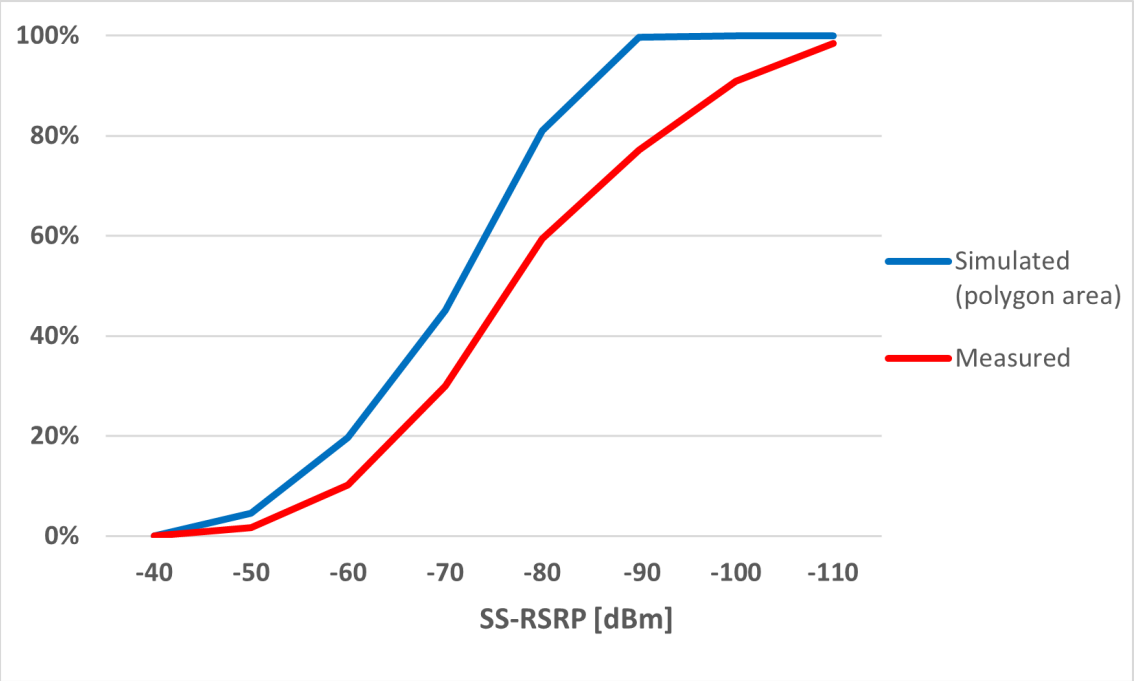

Figure 5.5. *Simulated vs measured cumulative SS-RSRP.*

Measurements results indicate that overall 5G coverage was good in the measured area and the lowest SS-RSRP values were -110 dBm, just like in the simulation results. Also, the SS-RSRP levels were -80 dBm or higher in 60% of the measured area. This value is calculated from Figure 5.4, which shows the percentage amount of total measured time to each SS-RSRP level. For example, the first level (Min -50 dBm Max -40 dBm 1.7%) means that the SS-RSRP level was less than or equal to -40 dBm 1.7% of the total measured time until the next level (<= -50 dBm). In other words, SS-RSRP levels were 1.7% of the total measured time between -40 dBm and -50 dBm. Simulated results were more optimistic than measured results, since 81% of the polygon area had SS-RSRP levels of -80 dBm or higher, while measured results only had 60 %. The measured cumulative SS-RSRP results are only taken from the polygon area, which is shown in Figure 4.9 to ensure that simulated results are compatible with the measured results. The simulated cumulative SS-RSRP graph matches quite well with the measured graph, but the simulated results are better, especially in the low SS-RSRP levels. This indicates that used propagation model in the simulation was too optimistic. Also, the antenna setup used in the simulation can have a positive impact on the simulation results, since the exact number of SSB beams and traffic beams along with patterns in those beams are unknown.

5.2.2 Measured SS-RSRQ

Measured SS-RSRQ levels from Busy-Hour scenario drive test are shown in Figure 5.6 and from Non Busy-Hour scenario drive test are shown in Figure 5.7. Measurements

results for both figures are similar and indicate that overall reference signal quality is excellent in the measured area. The probable cause for similarity in Figures 5.6 and 5.7 is that actual traffic amounts are quite close to each other in the Busy-Hour scenario and the Non Busy-Hour scenario. That would result in similar utilization of the cells and explain the similarity of the figures.

There are several reasons why Non Busy-Hour scenario measured from 9 am to 10 am can have the same traffic amount as the Busy-Hour scenario measured from 8 pm to 9 pm. Traditionally many people from suburban environments leave to work in the morning and return in the afternoon. However, since COVID-19 this is not necessarily the case anymore because remote working has increased significantly. Another reason could be that measurements were done in July, which is the popular month for people to be in summer holidays and resulting in more people staying home in the morning. Also since measurements were done within one day, there is no way of knowing was traffic in that particular day normal or abnormal. To determine that, many other measurement days would have been required, so the measurement sample size would be sufficient.

Figure 5.8 shows the cumulative SS-RSRQ on the simulated results and measured results for both traffic scenarios on the same graph.

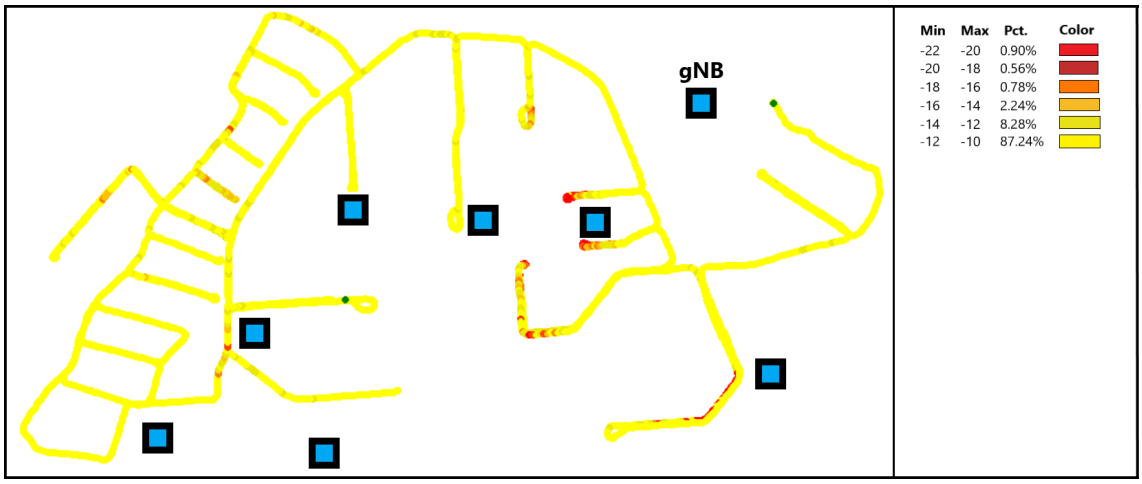

Figure 5.6. *Busy-Hour scenario SS-RSRQ measurement results in (dB).*

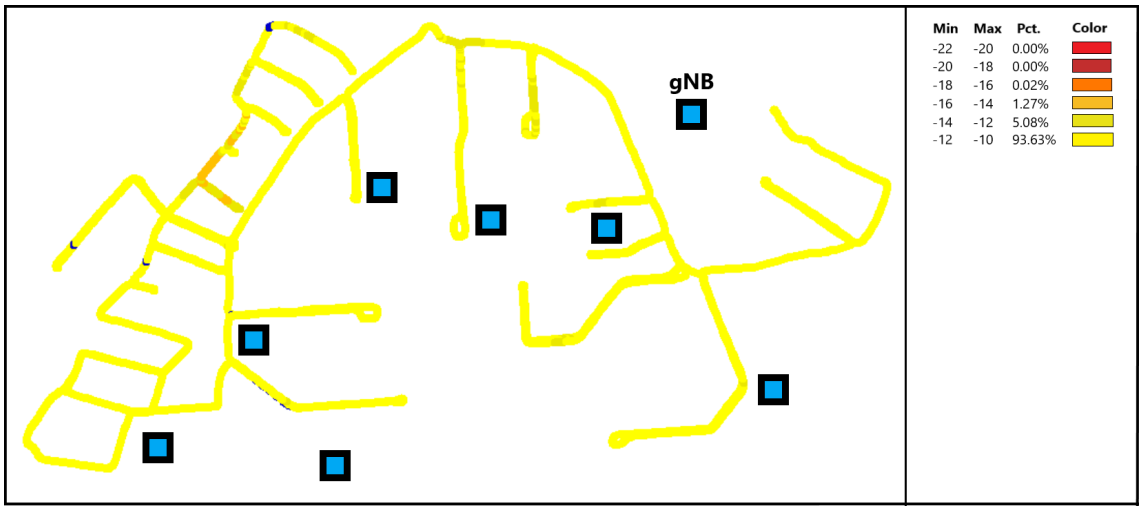

Figure 5.7. *Non Busy-Hour scenario SS-RSRQ measurement results in (dB).*

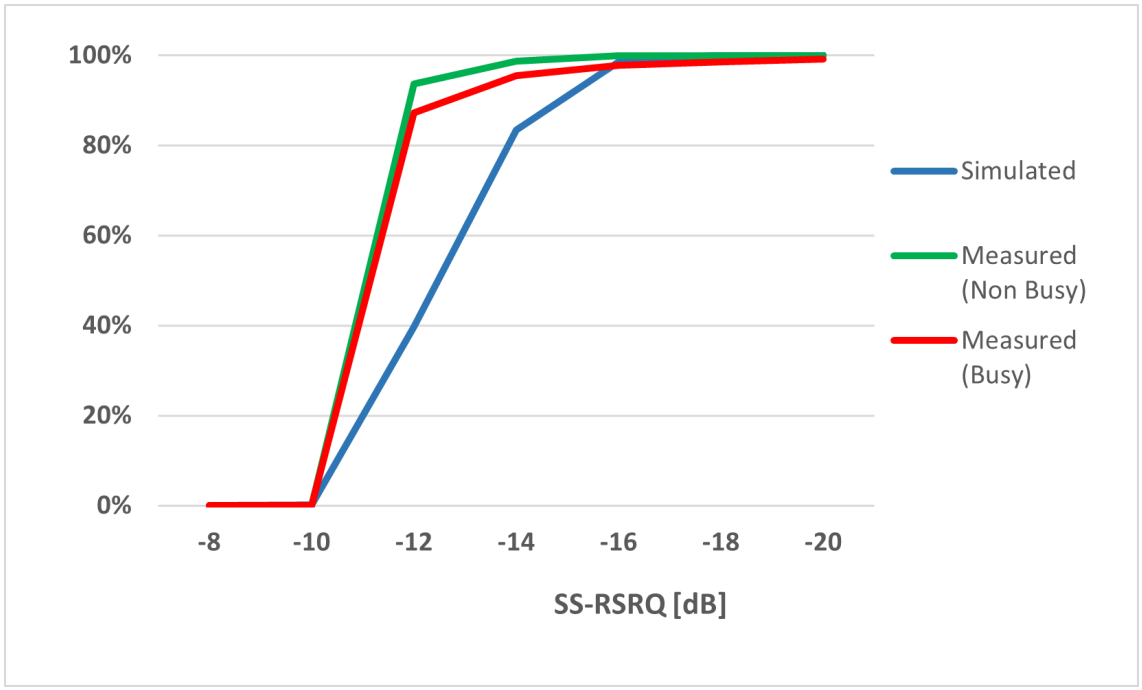

Figure 5.8. *Simulated vs measured cumulative SS-RSRQ on both traffic scenarios.*

In the Busy-Hour scenario, the SS-RSRQ levels were -12 dB or higher in 87% of the measured area, and the Non Busy-Hour scenario 94%. The values are calculated from the Figures 5.6 and 5.7 in the same way as the equivalent value in measured SS-RSRP. This differs quite from the simulated results, as shown in Figure 5.8. In the simulation, only 40% of the polygon area had SS-RSRQ levels of -12 dB or higher. This could be because the actual number of simultaneous users was lower in the field measurements than in the simulation. This would cause lower utilization of the cells and therefore lower RSSI values, which increases the SS-RSRQ values. Despite the fact that simulated traffic amounts in both scenarios were obtained from real network data, there could be a different definition

of what is meant by simultaneous users in ASSET Radio and network data. For example, ASSET Radio assumes that simulated users are constantly using the network, while users shown in network data possibly are not. This would explain why the traffic amount used in the simulation in both traffic scenarios seems high.

In the simulation cell utilization was quite high even with the Non-Busy hour traffic scenario. Another factor that can affect the SS-RSRQ values is overshooting from neighbor cells. Since the antenna setup in the simulation is not identical to the antenna setup in the field, there can be some overshooting happening in the simulation, which does not happen in the field.

5.2.3 Measured SS-SINR

Measured SS-SINR levels from the Busy-Hour scenario drive test are shown in Figure 5.9 and from Non Busy-Hour scenario drive test are shown in Figure 5.10. Measurements results for both figures are quite similar and indicate that overall signal quality is good in the measured area. As mentioned earlier, the similarity of the Figures 5.9 and 5.10 are probably caused by relatively same traffic amounts in the Busy-Hour scenario and Non Busy-Hour scenario. But unlike in SS-RSRQ results, there is a much bigger difference between Non Busy-Hour results and Busy-Hour results. This indicates that in the Busy-Hour measurements there was more DL interference, which is probably caused by an increased number of users. As the number of users increases, the interference from the own cell and other cells (co-channel interference) increases as well. Based on these measured SS-RSRQ and SS-SINR results, SS-SINR seems to be more sensitive to changes in radio conditions than SS-RSRQ.

Figure 5.11 shows the cumulative SS-SINR on the simulated results and measured results for both traffic scenarios on the same graph.

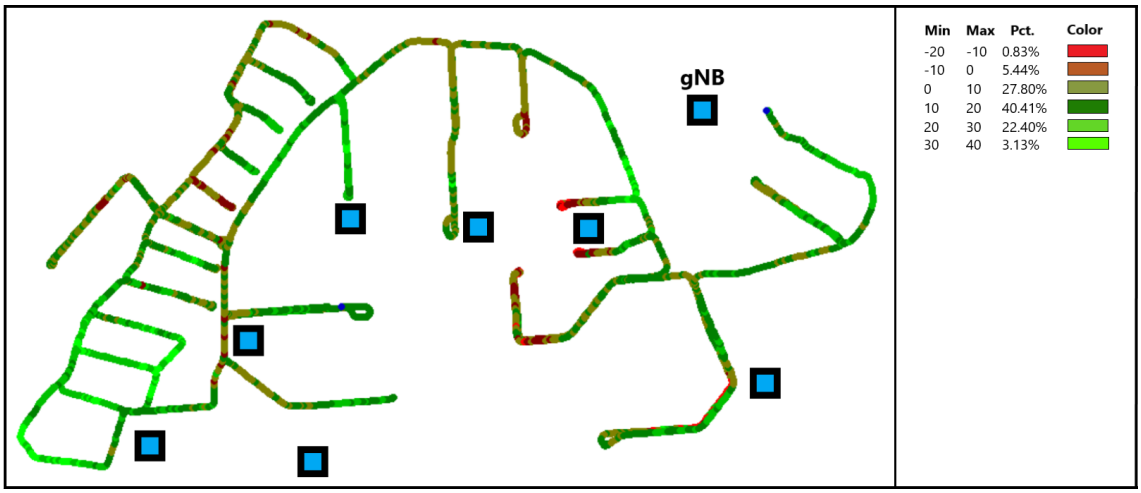

Figure 5.9. *Busy-Hour scenario SS-SINR measurement results in (dB).*

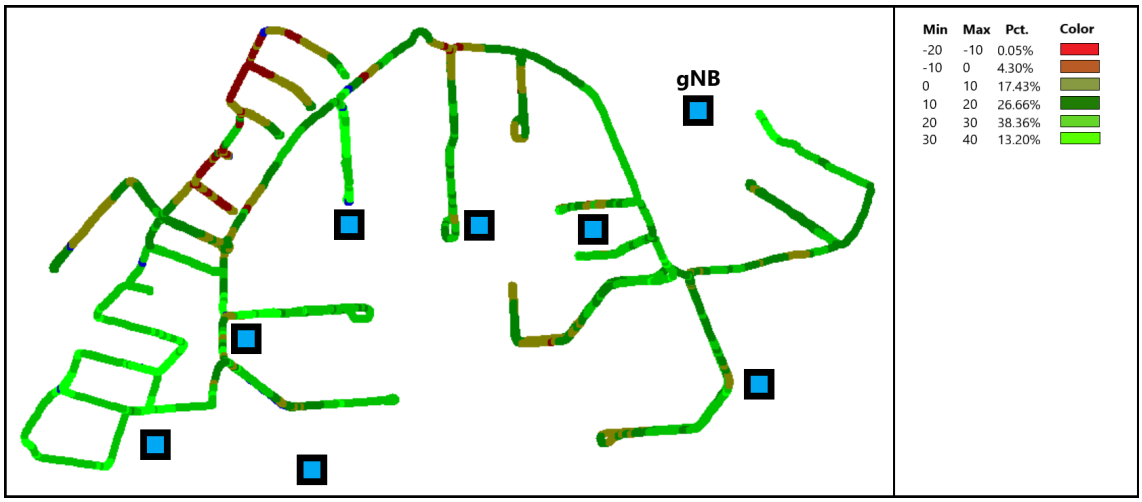

Figure 5.10. *Non Busy-Hour scenario SS-SINR measurement results in (dB).*

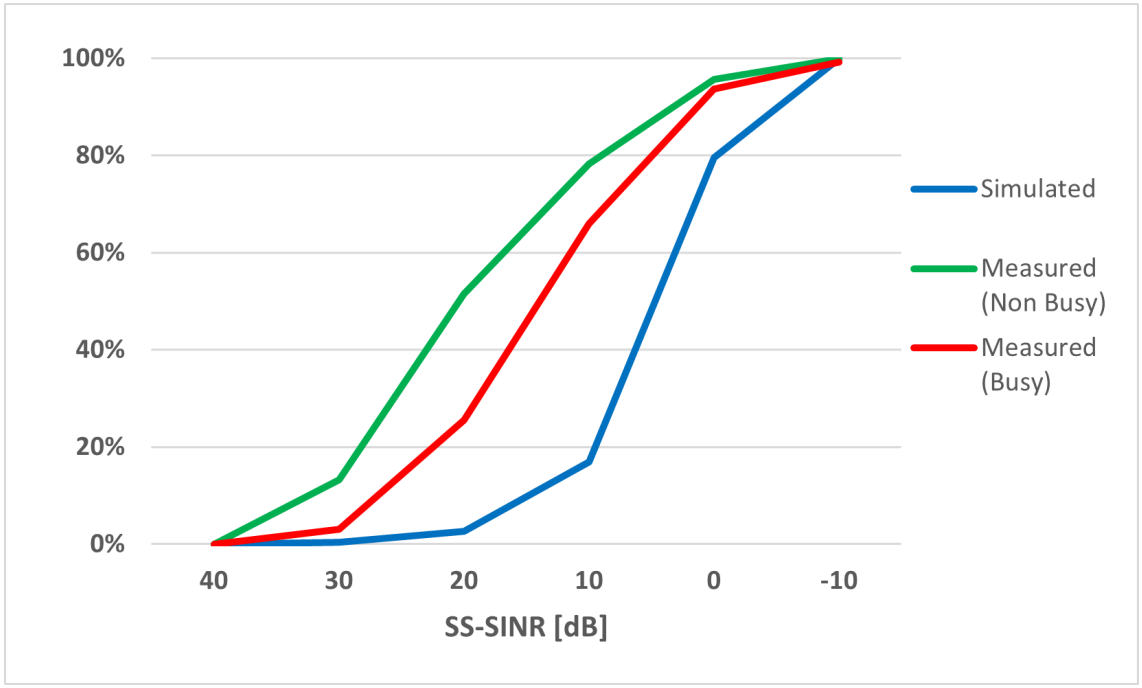

Figure 5.11. *Simulated vs measured cumulative SS-SINR on both traffic scenarios.*

In the Busy-Hour scenario, the SS-SINR levels were 13 dB or higher in 55% of the measured area, and the Non Busy-Hour scenario 75%. The values are calculated from the Figures 5.9 and 5.10 in the same way as the equivalent values in SS-RSRP and SS-RSRQ and also cross-referenced to Figure 5.11. The measured results differ quite a lot from the simulated results that are shown in Figure 5.11, since in the simulation only 15% of the simulated area had an SS-SINR level of 13 dB or higher. The probable reasons for this were the same as mentioned earlier, the actual number of simultaneous users was much lower in the field measurements than in the simulation. In the simulation, there was no notable difference in SS-SINR results between the Non Busy-Hour scenario and Busy-

Hour scenario simulations. This indicates that even only with 66 simultaneous users (Non Busy-Hour) SS-SINR results are already quite bad and increasing the number of simultaneous users beyond that does not have a notable effect on the results. Furthermore, since in the field measurements there was a notable difference between the Non Busy-Hour SS-SINR results and Busy-Hour SS-SINR results, it also supports our theory that the number of simultaneous users was lower in the field measurements than what was simulated.

5.2.4 Measured user throughput

Measured user throughput can not be directly compared to simulated user throughput, since measurements were done in the NSA 5G network, while the simulation is purely SA 5G network. Measured user throughput in an NSA 5G network is a combination of LTE Physical Downlink Shared Channel/Physical Uplink Shared Channel (PDSCH/PUSCH) throughput and 5G PDSCH/PUSCH throughput. To compare measured user throughput to simulated user throughput, LTE PDSCH/PUSCH throughput needs to be excluded from the results. In addition to that, PDSCH/PUSCH throughput is experienced at the PHY, while user throughput is experienced at the application layer. This also needs to be taken into account when calculating measured user throughput, which originates only from 5G PDSCH/PUSCH throughput.

The average 5G user application throughput was calculated in several steps. At first, the average LTE + 5G user application throughput was calculated by taking the total sum of HTTP transfer data rates and dividing it by the total number of HTTP transfer sessions. Next, the average of LTE PDSCH/PUSCH throughput and 5G PDSCH/PUSCH throughput were taken from all the HTTP transfer sessions and summed together to get the average LTE + 5G PDSCH/PUSCH throughput. This average LTE + 5G PDSCH/PUSCH throughput is compared to the average LTE + 5G user application throughput to know how much throughput is lost between the PHY and the application layer. Finally, when the estimation of throughput losses between different layers is known, the average 5G user application throughput can be calculated by subtracting the throughput losses from 5G PDSCH/PUSCH throughput.

Table 5.1 shows the average DL/UL throughput in the PHY and application (APP) layer for both traffic scenarios and throughput losses between layers in (Mbit/s). Figures 5.12 and 5.13 show the measured DL and UL average 5G user application throughput results and simulated throughput results with both traffic scenarios.

Table 5.1. *DL/UL throughput in (Mbit/s) at PHY and APP layer and layer losses.*

DL/UL	LTE (PHY)	5G (PHY)	LTE + 5G (PHY)	LTE + 5G (APP)	Losses	5G (APP)
DL (Non Busy)	248.57	545.89	794.46	660.86	16.82%	454.09
DL (Busy)	250.83	555.33	806.16	622.58	22.78%	428.85
UL (Non Busy)	49.95	50.87	100.82	83.54	17.14%	42.15
UL (Busy)	52.78	42.52	95.3	72.91	23.49%	32.53

It is worth mentioning that in Table 5.1 Non Busy-Hour scenario and Busy-Hour scenario LTE + 5G throughput in the PHY are close to each other for both DL and UL, but throughput losses are much higher in the Busy-Hour scenario resulting better application throughput in the Non Busy-Hour scenario. As mentioned earlier in the chapter 3, headers in each layer, iBLER value and TCP packet loss causes the difference between PHY throughput and application layer throughput. In this case, the results indicate that radio conditions were worse in the Busy-Hour scenario than in the Non Busy-Hour scenario, which increases the iBLER value. Also, in the evening the TCP packet loss may be higher than in the morning due to network congestion.

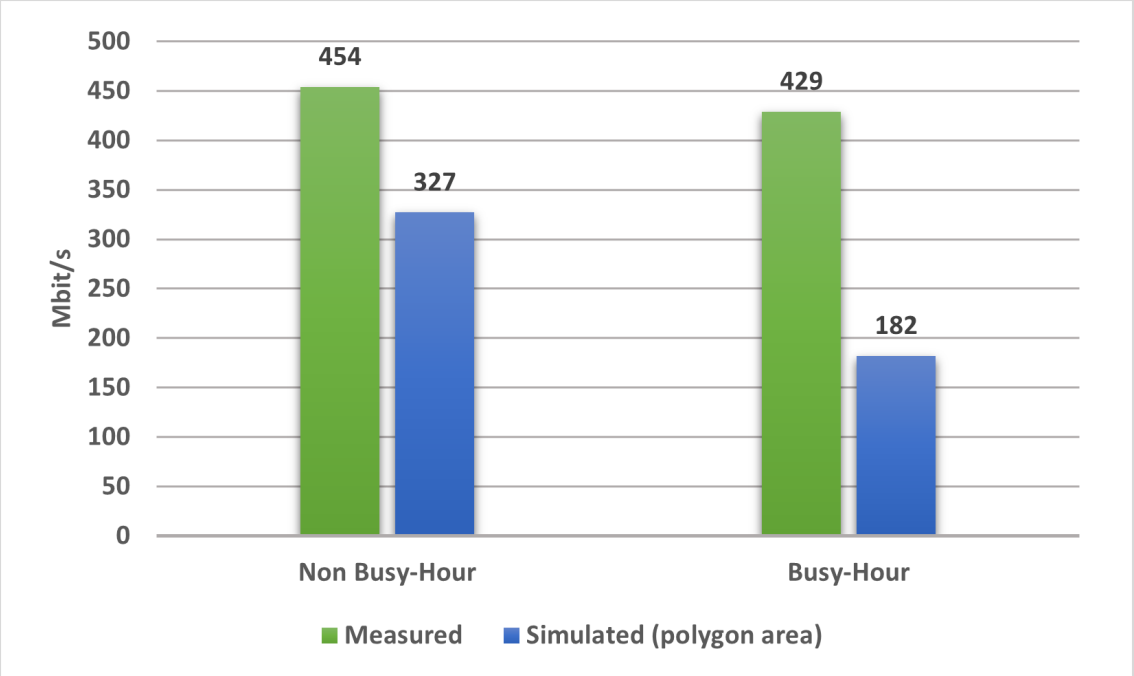

Figure 5.12. *Measured and simulated average DL 5G user throughput in both traffic scenarios.*

The measured average downlink user throughput in the Non Busy-Hour scenario was 454 Mbit/s and 429 Mbit/s in the Busy-Hour scenario. The Non Busy-Hour scenario did

not provide significantly higher downlink throughput than the Busy-Hour scenario, which also indicates that actual traffic amounts are close to each other in both traffic scenarios.

Compared to simulated results, measured downlink throughput was significantly higher in both traffic scenarios. In the Non Busy-Hour scenario measured downlink throughput was 39% higher than the simulated downlink throughput and in the Busy-Hour scenario measured downlink throughput was 236% higher. This also indicates that the actual number of simultaneous users was much lower in the field measurements than in the simulation.

Downlink average user application throughput was also measured with another OnePlus 9 phone, which had an unlimited data rate subscription. The measured downlink throughput in the Non Busy-Hour scenario was 463 Mbit/s and 423 Mbit/s in the Busy-Hour scenario. This indicates that unlimited data rate subscription had minimal to no effect on the downlink throughput.

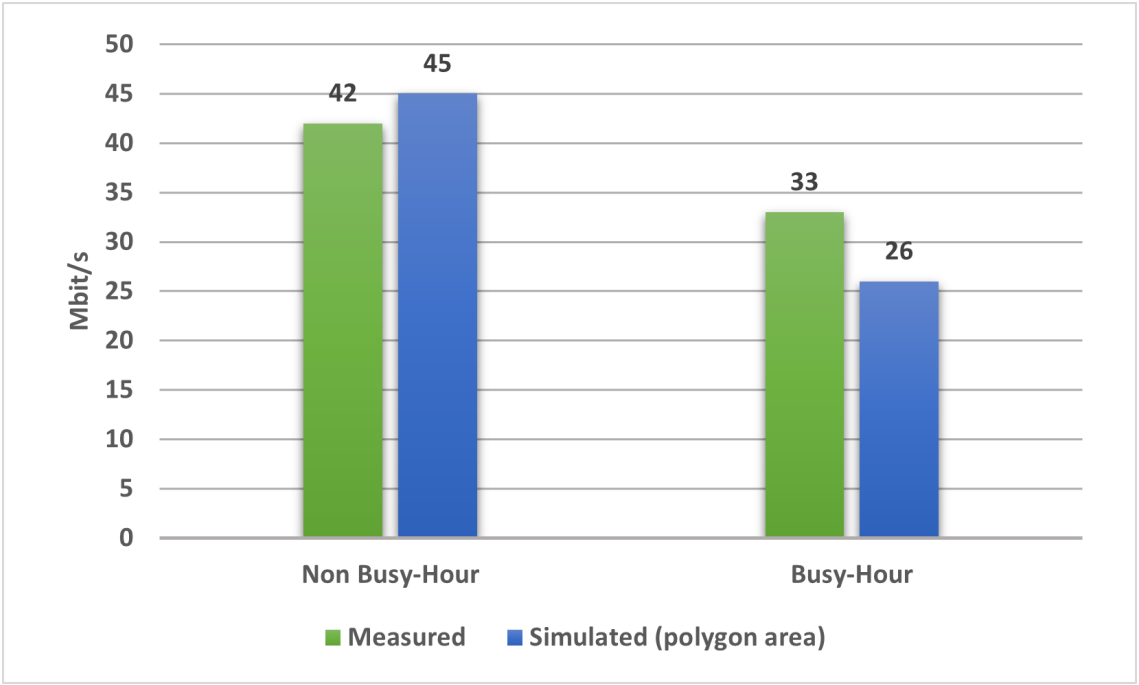

Figure 5.13. *Measured and simulated average UL 5G user throughput in both traffic scenarios.*

The measured average uplink user application throughput in the Non Busy-Hour scenario was 42 Mbit/s and 33 Mbit/s in the Busy-Hour scenario. The Non Busy-Hour scenario did not provide significantly higher uplink throughput than the Busy-Hour scenario, but the difference between traffic scenarios was more notable than in downlink throughput. This indicates that during measurements downlink utilization was quite the same in both traffic scenarios, while the uplink utilization was lower in the Non Busy-Hour scenario and resulted in notably better uplink throughput than in the Busy-Hour scenario.

Compared to simulated results, measured uplink throughput was smaller in the Non Busy-Hour scenario and higher in the Busy-Hour scenario. In the Non Busy-Hour scenario measured uplink throughput was 7% smaller than the simulated uplink throughput and in the Busy-Hour scenario measured uplink throughput was 27% higher. This indicates that compared to the simulation, relatively more resources were allocated to the downlink than the uplink during field measurements. The ratios between measured downlink user throughput and measured uplink user throughput were approximately 11:1 in the Non Busy-Hour scenario and 13:1 in the Busy-Hour scenario, which is notably higher than in the simulation.

Another OnePlus 9 phone, which had an unlimited data rate subscription gave 40 Mbit/s uplink throughput in the Non Busy-Hour scenario and 35 Mbit/s uplink throughput in the Busy-Hour scenario. Just like in the downlink direction, unlimited data rate subscription had minimal to no effect on the uplink throughput.

The 5G RAN model was also simulated with other traffic amounts than the Non Busy-Hour scenario (66 UEs) or Busy-Hour scenario (140 UEs) out of curiosity. At first, the simulation was done with many different traffic amounts that were lower than 66 UEs, to find the correct traffic amount that would lead to the same throughput results as the measured results in the Non Busy-hour scenario. Simulation done with 40 UEs gave average downlink user throughput of 457 Mbit/s and average uplink user throughput of 49 Mbit/s, which are close to the measured results. This indicates that the real number of simultaneous user in the field measurements were approximately 40 UEs, according to the 5G RAN model. The simulation was also done with only 1 UE, to know what throughput the user experiences in the empty network. In this simulation, the average downlink user throughput was 995 Mbit/s and the average uplink user throughput was 78 Mbit/s. Throughput in the downlink direction is almost maximum since ASSET Radio has a 1 Gbit/s limit but uplink throughput is quite low considering that the network is empty. The cause for this is that terminal has only 2 TX elements compared to its 4 RX elements and there is a 4:1 ratio between downlink and uplink slots. Those limit the uplink throughput dramatically, even when the network is empty. Based on downlink user throughput, uplink user throughput can be estimated when the slot ratio, antenna elements, and modulation are taken into account: If downlink user throughput is 995 Mbit/s with a 4:1 slot ratio, uplink user throughput is 995 Mbit/s * 20% = 199 Mbit/s. Then given the fact that downlink uses ideally 4 independent data streams while uplink uses only 2 independent data streams, uplink throughput is 199 Mbit/s * 50% = 99.5 Mbit/s and taking the modulation into account (DL 256QAM = 8 bits, and UL 64QAM = 6 bits) uplink throughput estimation is: (6/8)*99.5 Mbit/s = 75 Mbit/s.

5.3 User throughput distribution across cells

Both simulated and measured user throughput varied notably, depending on the serving cell. Figure 5.14 shows DL and UL user throughput distribution on polygon area simulation in the Non Busy-Hour scenario. Each cell from the simulation has a unique identity number between 1 and 24 since the simulation contained 24 cells.

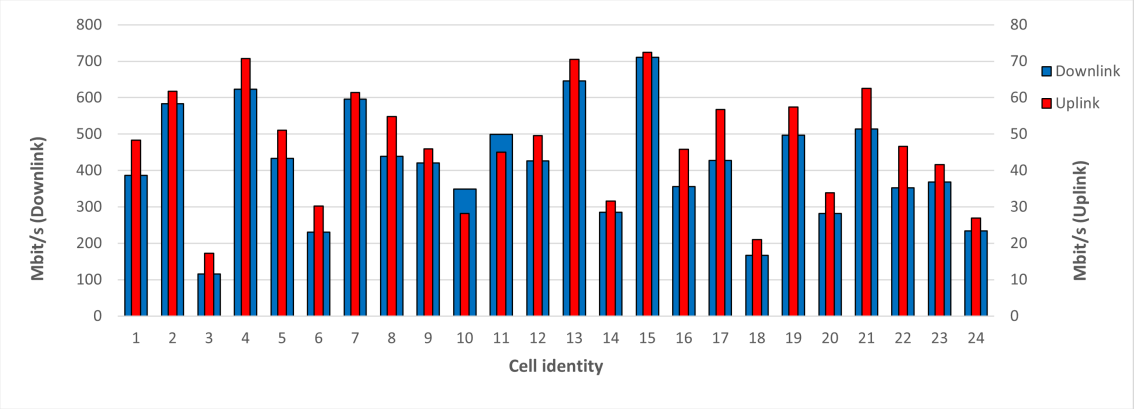

Figure 5.14. *DL/UL user throughput distribution across cells (Non Busy-Hour).*

The ratio between simulated DL and UL user throughput in each cell is similar, approximately 8:1, which indicates that there is a high correlation between DL and UL user throughput. The average ratio between DL and UL user throughput in this Figure 5.14 is higher than the one calculated from simulated average user throughput in subsection 4.4.4 because here each cell has equal weight in terms of traffic which distorts the ratio. Cell identity ’3’ experienced the lowest throughput values (DL 116 Mbit/s and UL 17 Mbit/s), while cell identity ’15’ experienced the highest throughput values (DL 711 Mbit/s and UL 72 Mbit/s). The massive difference in throughput values between cell identities ’3’ and ’15’ is directly linked to served users in that cell, which was tenfold in cell identity ’3’. Figures 5.15 and 5.16 shows simulated vs measured DL and UL user throughput distribution. Simulated DL and UL user throughput distribution is the same as shown in the previous Figure.

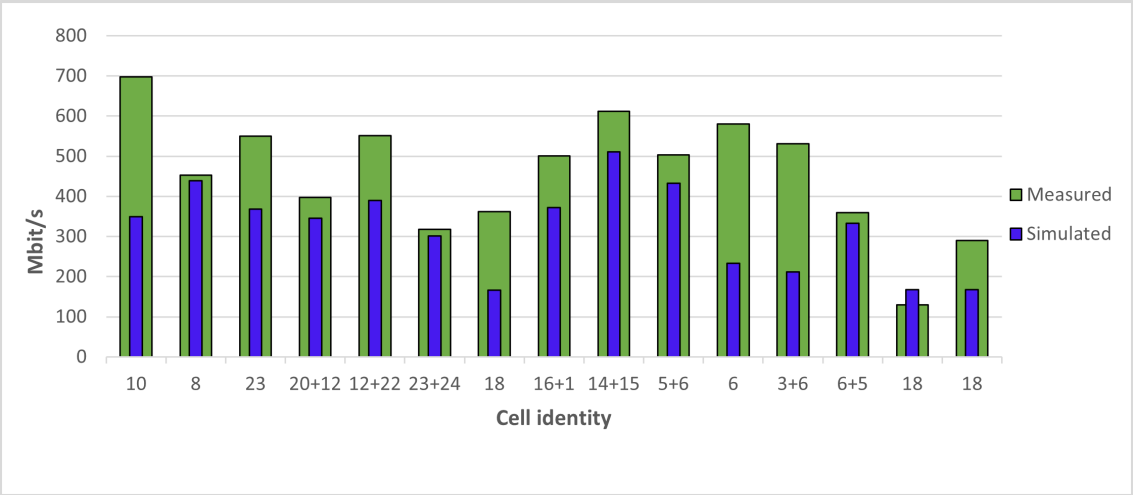

Figure 5.15. *Simulated vs measured DL user throughput distribution.*

Figure 5.15 shows the average DL user throughput on each HTTP transfer session and serving cell(s) during that session vs simulated average DL throughput on the same cell. In many HTTP transfer sessions, there are two serving cells, meaning that UE changed the serving cell during downloading. For example, the fourth HTTP transfer session marked as "20+12" means that the download started in the cell identity ’20’ and ended in the cell identity ’12’. In cases where downloading has happened in multiple cells, the simulated DL user throughput was calculated by taking the weighted average on those cells. Weights were determined by the cell’s serving time with respect to the total HTTP transfer session time. Some minor correlations can be seen between simulated and measured DL user throughput distribution, but given the fact that simulated average DL user throughput was 39% lower than measured, correlation is harder to distinguish. It is worth mentioning that downloading only used 15 different serving cells out of 24 during field measurements. This can be explained by looking at the topology in Figure 4.9, where 5 cells do not have coverage to the polygon area. The rest 4 cells were probably skipped during driving when downloading did not occur or some other cells were a better fit to be UEs serving cells. In the field measurements, the cell identity ’18’ experienced the lowest throughput value of 130 Mbit/s, while the cell identity ’10’ experienced the highest throughput value of 697 Mbit/s. The lowest and highest value are the same magnitudes as the ones in the simulated DL user throughput distribution. However, those happened on different cell identities.

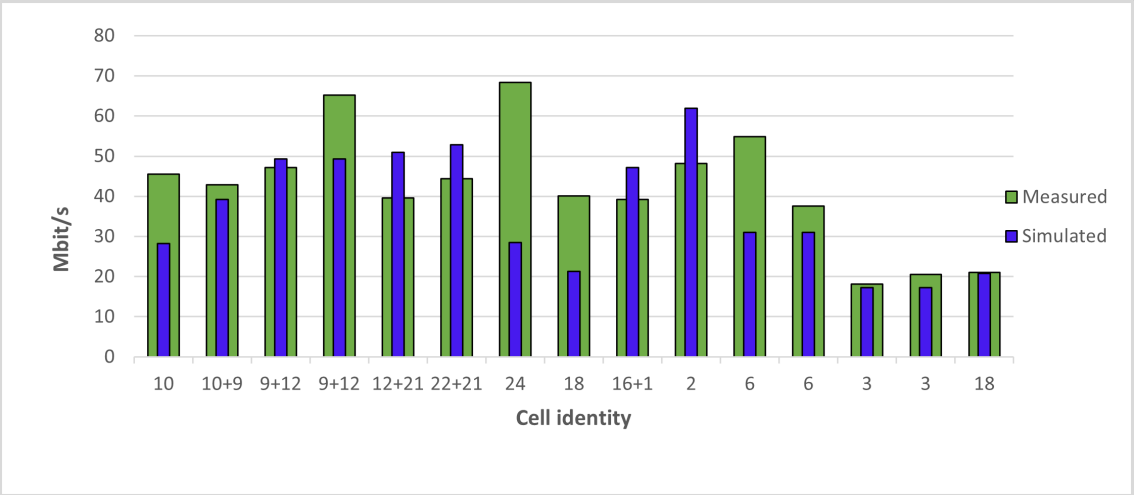

Figure 5.16. *Simulated vs measured UL user throughput distribution.*

Figure 5.15 shows the average UL user throughput on each HTTP transfer session and serving cell(s) during that session vs simulated average UL throughput on the same cell. In cases where uploading has happened in multiple cells, the simulated UL user throughput was calculated in a similar way as the simulated DL user throughput. The correlation between simulated and measured UL user throughput distribution is more obvious than in DL distribution since the simulated average UL user throughput was much closer to the measured UL user throughput. Similar to DL field measurements, only 15 serving cells out of 24 were used. In the field measurements, the cell identity ’3’ experienced the lowest throughput value of 18 Mbit/s, while the cell identity ’24’ experienced the highest throughput value of 68 Mbit/s. In the simulation cell identity ’3’ also experienced the the lowest UL throughput value of 17 Mbit/s. Similar to downloading, uploading also used only 15 different serving cells out of 24, but the serving cells were not identical to the ones used in downloading. This can be explained by looking at the measurement script in Figure 5.2, where there is a 20-second wait between uploading and downloading. During that time it is probable that UE has moved to another cell’s coverage area when field measurements are done with a car.

5.3.1 Results summary

This subsection summarises the results from the whole simulation area, polygon-covered simulation area, and field measurements area. Results from the whole simulation area are also displayed here to highlight the difference in results between the whole area simulation and the polygon area simulation. Figures 5.17, 5.18 and 5.19 shows the cumulative SS-RSRP, SS-RSRQ and SS-SINR results on the whole area simulation, polygon area simulation and measured area on the same graph. Figures 5.20 and 5.22 show the average DL and UL 5G user throughput on the whole simulation area, polygon simulation area, and measured area on both traffic scenarios.

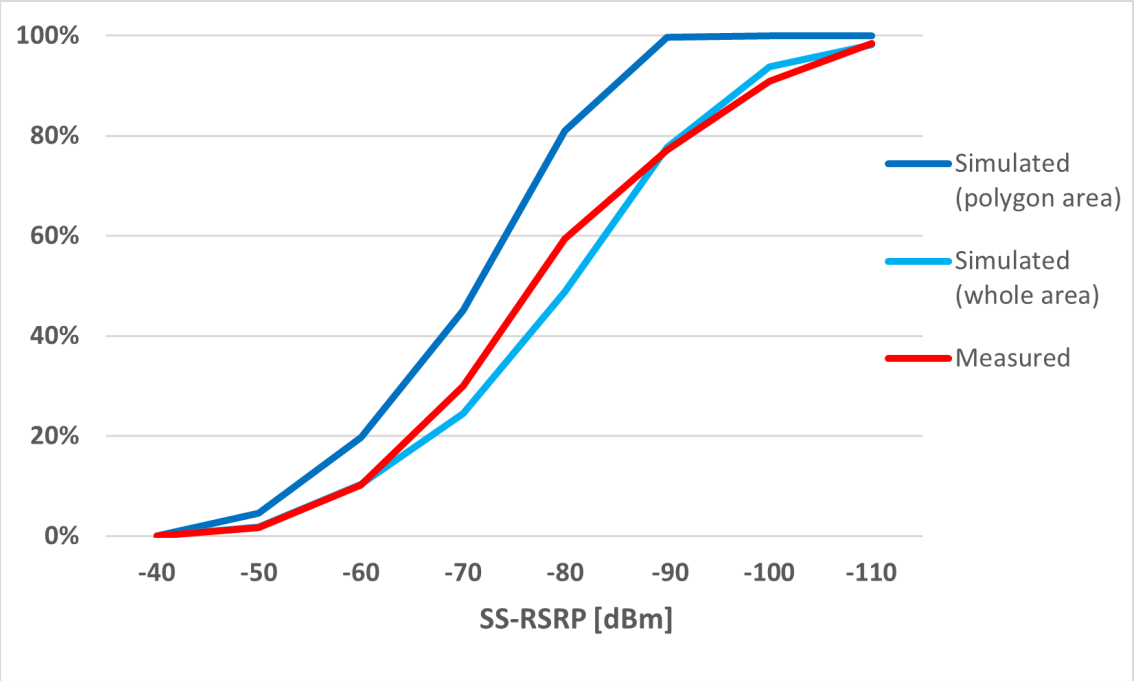

Figure 5.17. *Cumulative SS-RSRP on the whole simulation area, polygon simulation area, and measured area.*

In Figure 5.17 there is a substantial difference in the SS-RSRP levels between the whole simulation area and the polygon simulation area. Statistics show that 81% in the polygon simulation area had SS-RSRP levels of -80 dBm or higher, while the whole simulation area only had 49%. This sounds plausible since the whole simulation area takes into account all the low-level SS-RSRP locations, which are shown in the heat map Figure 4.11, while the polygon simulation area does not have nearly as many low SS-RSRP level locations.

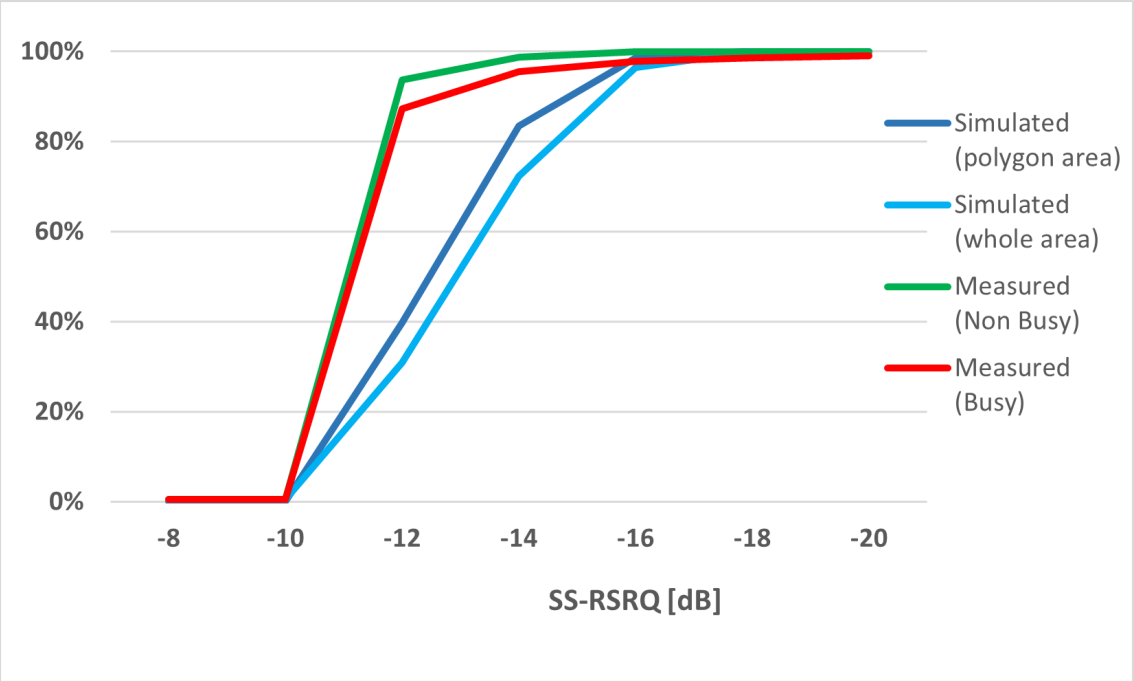

Figure 5.18. *Cumulative SS-RSRQ on the whole simulation area, polygon simulation area, and measured area on both traffic scenarios.*

In Figure 5.18 there is a difference in the SS-RSRQ levels between the whole simulation area and polygon simulation area, but not as notable as in SS-RSRP results. Statistics show that 40% in the polygon simulation area had SS-RSRQ levels of -12 dBm or higher, while the whole simulation area had 31%. The heat map Figure 4.13 shows that SS-RSRQ levels are not so sensitive to the increasing distance from the base station unlike SS-RSRP levels, which explains why the difference between whole area results and polygon area results are close to each other.

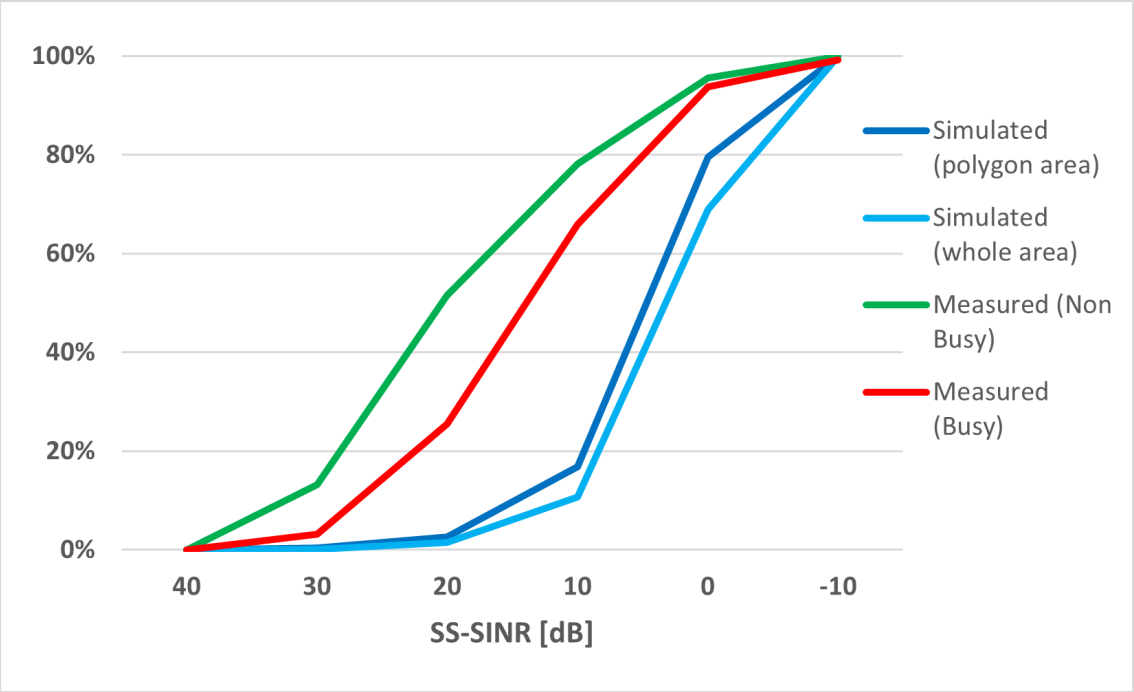

Figure 5.19. *Cumulative SS-SINR on the whole simulation area, polygon simulation area, and measured area on both traffic scenarios.*

In Figure 5.19 the difference between the whole simulation area SS-SINR results and polygon simulation area SS-SINR results are similar to SS-RSRQ results. Statistics show that 15% in the polygon simulation area had SS-SINR levels of -13 dBm or higher, while the whole simulation area had 9%. The heat map Figure 4.15 shows that SS-SINR levels are highly sensitive to the increasing distance from the base station and even the majority of the polygon area experiences low SS-SINR levels, despite being relatively close base stations. This explains why the difference between whole area results and polygon area results are close to each other.

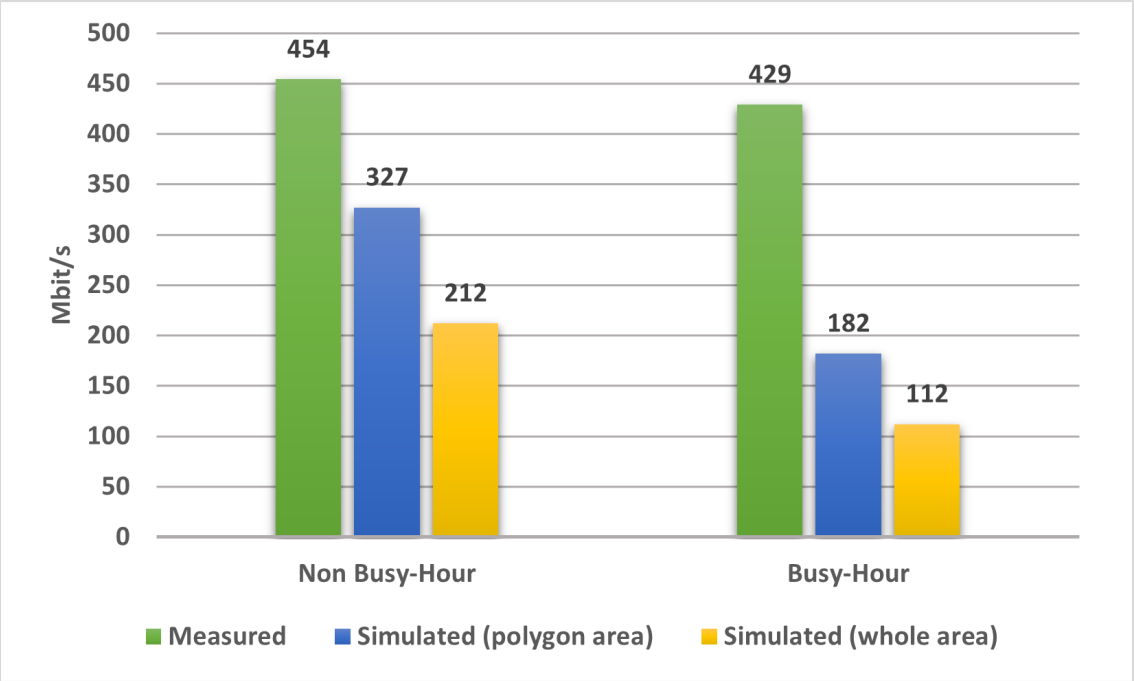

Figure 5.20. *Average DL 5G user throughput on the whole simulation area, polygon simulation area, and measured area on both traffic scenarios.*

In Figure 5.20 the difference in average DL 5G user throughput between the whole simulation area and polygon simulation area is substantial. The polygon simulation area experienced 54% higher DL user throughput than the whole simulation area in the Non Busy-Hour scenario and 62% higher in the Busy-Hour scenario. This indicates that location has a high impact on the DL user throughput and emphasizes the fact, that the simulated area must match with the measured area to have comparable results. The location dependence on DL user throughput can also be seen in Figure 5.21, which shows achievable DL 5G user throughput on the whole simulation area.

Figure 5.21. *Achievable DL 5G user throughput on the whole simulation area in (Mbit/s).*

Figure 5.21 shows the theoretical maximum DL user throughput that the user can achieve

with this 5G RAN model. It assumes perfect radio conditions, an empty network, and no limiting factor on the maximum service rate. In the best locations achievable DL 5G user throughput is 1.5—1.7 Gbit/s, while in the bad locations it is 0.7–252 Mbit/s. The polygon simulation area has notably better achievable user throughput levels than the whole simulation area. This explains why there is such a big difference in the average user throughput between the polygon simulation area and the whole simulation area. It is worth mentioning that the bad locations shown in this simulation are probably covered by other cells in real-life, which are outside of this simulation area and would experience better radio conditions.

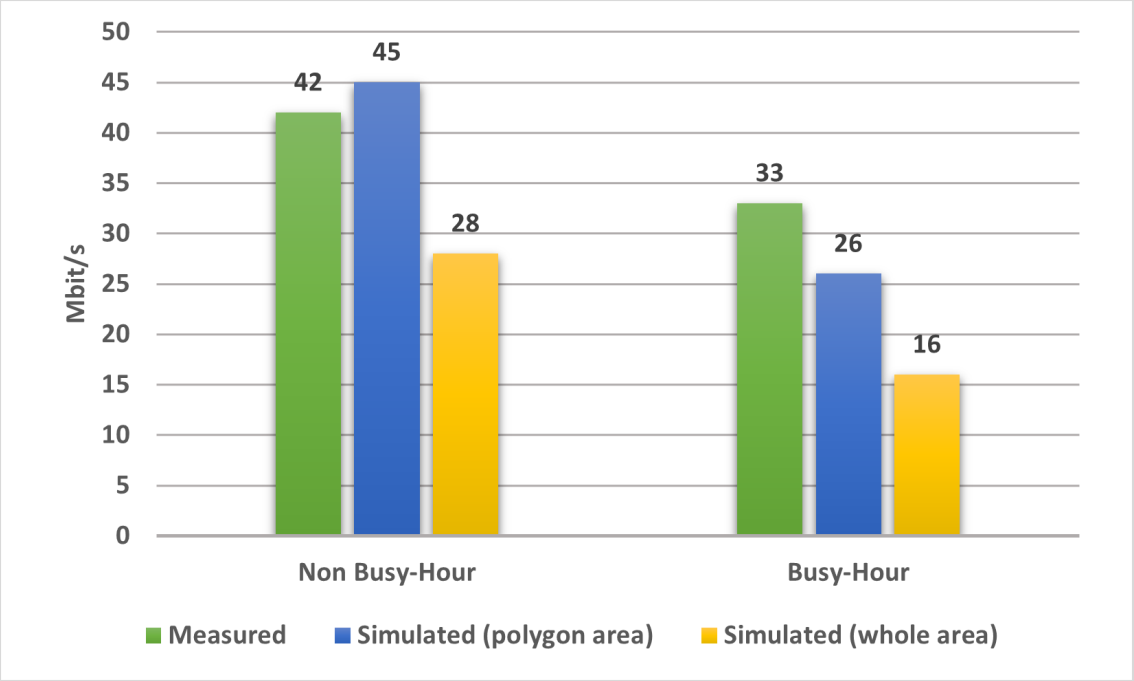

Figure 5.22. *Average UL 5G user throughput on the whole simulation area, polygon simulation area, and measured area on both traffic scenarios.*

In Figure 5.22 the difference in average UL 5G user throughput between the whole simulation area and polygon simulation area is also substantial. The polygon simulation area experienced 73% higher user throughput than the whole simulation area in the Non Busy-Hour scenario and 75% higher in the Busy-Hour scenario. The location has a similar impact on the UL user throughput, which it had on the DL user throughput. The achievable UL 5G user throughput heat map had a similar distribution of achievable throughput, only with lower values.

6. CONCLUSIONS

Building an accurate 5G RAN model in ASSET Radio that would give the same simulated results as field measurement results on the equivalent real-life 5G RAN, requires an extensive amount of exact information from that 5G network. Even minor discrepancies in traffic amounts, traffic distributions, antenna configurations, etc. between the 5G RAN model and real-life 5G RAN can cause substantial differences in the results. Additionally, ASSET Radio has its limitations such as the ability to only perform static simulations, a maximum service rate of 1 Gbit/s, and a limited number of different propagation models.

Field measurement equipment, setup, and measurement techniques have obvious impacts on the measured results and to get reliable results, several factors need to be taken into account such as measurement route, speed, script, and time on a measured day along with the period during that year. Also, unexpected challenges that can affect field measurement results such as the phone's inability to connect to the 5G network and mass events near were made known. It was shown that field measurement results between the Non Busy-Hour traffic scenario, which was measured at 9 am, and the Busy-Hour traffic scenario, which was measured at 8 pm were similar and the actual number of simultaneous users during those measurements were close to each other. This can be caused by several reasons such as increased remote working due to COVID-19, the summer holiday period, or abnormal traffic during that measurement day.

Measured results in both traffic scenarios were better than simulated results, except for polygon area uplink user throughput in Non Busy-Hour scenario and SS-RSRP results. This implies that the number of simultaneous users was lower in the field measurements than in the simulation since the incorrect traffic amount in the 5G RAN model is the most probable cause for discrepancies in the results. The propagation model used in the simulation was a little optimistic since SS-RSRP results are not affected by traffic amount. Since the measured throughput results in an NSA 5G network were a combination of LTE and 5G throughput and simulated throughput results in a SA 5G network were 5G throughput only, the measured throughput was not directly comparable to the simulated throughput. It was shown that from the measured downlink throughput results approximately 31% were LTE throughput and from the measured uplink throughput results, approximately 53% were LTE throughput. Both in the simulation and the field measurements, user throughput varied a lot depending on the serving cell. Some correlations

were found between simulated and measured user throughput distribution across different cells indicating that with a correct traffic amount and traffic distribution even accurate cell-level analysis on user throughput would be possible.

The simulated results in the polygon area, which represented the field measurements area were significantly better than the simulated results in the whole simulation area. This highlights the importance that the simulated area must match with the measured area, to have comparable results. Overall, ASSET Radio simulation results seem highly plausible and analysis indicates that if the 5G RAN model would be identical to the equivalent real-life 5G RAN, the simulation results would be highly similar to the measured results. Unfortunately, in this case, it can not be indisputably proven, since the used antenna setup in the simulation was different and the actual number of simultaneous users in the field measurements was unknown. This thesis can be used to do further research on the system-level simulation of 5G networks and use field measurements to verify the accuracy of that simulation. Furthermore, the same concept can be implemented to do system-level simulation on a more complex network, that would include for example all the previous-generation technologies.

REFERENCES

[1] Series, M. IMT Vision–Framework and overall objectives of the future development of IMT for 2020 and beyond. *Recommendation ITU* 2083 (2015), p. 12.

[2] Abhayawardhana, V., Wassell, I., Crosby, D., Sellars, M. and Brown, M. Comparison of empirical propagation path loss models for fixed wireless access systems. *2005 IEEE 61st Vehicular Technology Conference*. Vol. 1. IEEE. 2005, pp. 73–77.

[3] Mahmud, H. Cellular mobile technologies (1G to 5G) and massive MIMO. *Int. J. Sci. Res* 8.7 (2019), pp. 929–937.

[4] Korhonen, J. *Introduction to 3G mobile communications*. Artech House, 2003.

[5] Bhandarkar, S. and Kammar, R. 4G Technology. (Jan. 2016). DOI: 10.5281/zenodo.158935.

[6] Sood, R. and Garg, A. Digital society from 1G to 5G: a comparative study. *International Journal of Application or Innovation in Engineering & Management (IJAIEM)* 3.2 (2014), pp. 186–193.

[7] Chochliouros, I. P., Yi, N., Spiliopoulou, A. S., Kostopoulos, A., Gomes, N., Herzog, U., Chen, T., Dardamanis, A., Segou, O., Assimakopoulos, P. et al. Enhanced Mobile Broadband as Enabler for 5G: Actions from the Framework of the 5G-DRIVE Project. *IFIP International Conference on Artificial Intelligence Applications and Innovations*. Springer. 2019, pp. 31–45.

[8] Ghosh, A. *5G New Radio (NR): Physical Layer Overview and Performance. IEEE Communication Theory Workshop*.

[9] 3GPP. *System architecture for the 5G system*. Technical Specification (TS) 23.501. Version 15.2.0. 3rd Generation Partnership Project (3GPP), 2018. URL: https://www.etsi.org/deliver/etsi_ts/123500_123599/123501/15.02.00_60/ts_123501v150200p.pdf.

[10] Samsung. Technical Report, 5G Core Vision. 1 (2019), pp. 4–7.

[11] 3GPP. *Digital cellular telecommunications system (Phase 2+) (GSM); Universal Mobile Telecommunications System (UMTS); LTE; 5G;* Technical Report (TR) 21.915. Version 15.0.0. 3rd Generation Partnership Project (3GPP), 2017. URL: https://www.etsi.org/deliver/etsi_tr/121900_121999/121915/15.00.00_60/tr_121915v150000p.pdf.

[12] 3GPP. *5G; NR; User Equipment (UE) radio transmission and reception; Part 1: Range 1 Standalone*. Technical Specification (TS) 38.101-1. Version 15.3.0. 3rd Generation Partnership Project (3GPP), 2018, p. 16. URL: https://www.etsi.

org/deliver/etsi_ts/138100_138199/13810101/15.03.00_60/ts_13810101v150300p.pdf.

[13] 3GPP. *5G; NR; Overall description; Stage-2*. Technical Specification (TS) 38.300. Version 15.8.0. 3rd Generation Partnership Project (3GPP), 2018, p. 18. URL: https://www.etsi.org/deliver/etsi_ts/138300_138399/138300/15.08.00_60/ts_138300v150800p.pdf.

[14] 3GPP. *5G; NR; Physical channels and modulation*. Technical Specification (TS) 38.211. Version 15.2.0. 3rd Generation Partnership Project (3GPP), 2018, pp. 9–16. URL: https://www.etsi.org/deliver/etsi_ts/138200_138299/138211/15.02.00_60/ts_138211v150200p.pdf.

[15] Lin, X., Li, J., Baldemair, R., Cheng, J.-F. T., Parkvall, S., Larsson, D. C., Koorapaty, H., Frenne, M., Falahati, S., Grovlen, A. et al. 5G new radio: Unveiling the essentials of the next generation wireless access technology. *IEEE Communications Standards Magazine* 3.3 (2019), pp. 30–37.

[16] Hoomod, H. K., Al-Mejibli, I. and IssaJabboory, A. Optimizing SOM for cell towers distribution. *2017 Annual Conference on New Trends in Information & Communications Technology Applications (NTICT)*. IEEE. 2017, pp. 138–143.

[17] Mawjoud, S. Evaluation of power budget and Cell coverage Range in Cellular GSM System. *Al-Rafidain Engineering Journal (AREJ)* 16.1 (2008), pp. 37–47.

[18] Sharma, S. *Wireless & Cellular Communications*. SK Kataria and Sons, 2009.

[19] Elechi, P. and Otasowie, P. O. Comparison of empirical path loss propagation models with building penetration path loss model. *International Journal on Communications Antenna and Propagation* 2016 (2016), pp. 116–123.

[20] Damosso, E., Correia, L. M. et al. COST action 231: Digital mobile radio towards future generation systems: Final report. *European commission* (1999).

[21] Anderson, H. R. *Fixed broadband wireless system design*. John Wiley & Sons, 2003.

[22] Milanovic, J., Rimac-Drlje, S. and Bejuk, K. Comparison of propagation models accuracy for WiMAX on 3.5 GHz. *2007 14th IEEE international conference on electronics, circuits and systems*. IEEE. 2007, pp. 111–114.

[23] Hoppe, R., Wolfle, G. and Landstorfer, F. Measurement of building penetration loss and propagation models for radio transmission into buildings. *Gateway to 21st Century Communications Village. VTC 1999-Fall. IEEE VTS 50th Vehicular Technology Conference (Cat. No. 99CH36324)*. Vol. 4. IEEE. 1999, pp. 2298–2302.

[24] Hata, M. Empirical formula for propagation loss in land mobile radio services. *IEEE transactions on Vehicular Technology* 29.3 (1980), pp. 317–325.

[25] Popoola, S. I. and Oseni, O. F. Empirical path loss models for GSM network deployment in Makurdi, Nigeria. *International Refereed Journal of Engineering and Science* 3.6 (2014), pp. 85–94.

[26] TEOCO. ASSET, User Reference Guide. Version 2021 Q2. (2021), p. 375.

[27] Yun, Z. and Iskander, M. F. Ray tracing for radio propagation modeling: Principles and applications. *IEEE access* 3 (2015), pp. 1089–1100.

[28] 3GPP. *5G; NR; Physical layer measurements*. Technical Specification (TS) 38.215. Version 16.2.0. 3rd Generation Partnership Project (3GPP), 2020, pp. 9–13. URL: https://www.etsi.org/deliver/etsi_ts/138200_138299/138215/16.02.00_60/ts_138215v160200p.pdf.

[29] 3GPP. *5G; NR; User Equipment (UE) radio access capabilities*. Technical Specification (TS) 38.306. Version 15.2.0. 3rd Generation Partnership Project (3GPP), 2018, pp. 6–7. URL: https://www.etsi.org/deliver/etsi_ts/138300_138399/138306/15.02.00_60/ts_138306v150200p.pdf.

[30] Koziol, D. and Määttänen, H.-L. Network Architecture and NR Radio Protocols. *5G New Radio: A Beam-based Air Interface* (2020), pp. 25–93.

[31] 3GPP. *5G; NR; Medium Access Control (MAC) protocol specification*. Technical Specification (TS) 38.321. Version 15.3.0. 3rd Generation Partnership Project (3GPP), 2018, p. 11. URL: https://www.etsi.org/deliver/etsi_ts/138300_138399/138321/15.03.00_60/ts_138321v150300p.pdf.

[32] 3GPP. *5G; NR; Radio Link Control (RLC) protocol specification*. Technical Specification (TS) 38.322. Version 15.3.0. 3rd Generation Partnership Project (3GPP), 2018, p. 12. URL: https://www.etsi.org/deliver/etsi_ts/138300_138399/138322/15.03.00_60/ts_138322v150300p.pdf.

[33] 3GPP. *5G; NR; Packet Data Convergence Protocol (PDCP) specification*. Technical Specification (TS) 38.323. Version 16.4.0. 3rd Generation Partnership Project (3GPP), 2021, p. 12. URL: https://www.etsi.org/deliver/etsi_ts/138300_138399/138323/16.04.00_60/ts_138323v160400p.pdf.

[34] 3GPP. *LTE; 5G; Evolved Universal Terrestrial Radio Access (E-UTRA) and NR; Service Data Adaptation Protocol (SDAP) specification*. Technical Specification (TS) 37.324. Version 16.2.0. 3rd Generation Partnership Project (3GPP), 2021, p. 9. URL: https://www.etsi.org/deliver/etsi_ts/137300_137399/137324/16.02.00_60/ts_137324v160200p.pdf.

[35] 3GPP. *5G; NR; Radio Resource Control (RRC);* Technical Specification (TS) 38.331. Version 15.2.1. 3rdGeneration Partnership Project (3GPP), 2018, pp. 18–19. URL: https://www.etsi.org/deliver/etsi_ts/138300_138399/138331/15.02.01_60/ts_138331v150201p.pdf.

[36] 3GPP. *5G; Non-Access-Stratum (NAS) protocol for 5G System (5GS); Stage 3*. Technical Specification (TS) 24.501. Version 16.5.1. 3rdGeneration Partnership Project (3GPP), 2020, p. 36. URL: https://www.etsi.org/deliver/etsi_ts/124500_124599/124501/16.05.01_60/ts_124501v160501p.pdf.

[37] 3GPP. *5G; Study on 5G NR User Equipment (UE) application layer data throughput performance*. Technical Report (TR) 37.901-5. Version 16.8.0. 3rdGeneration Partnership Project (3GPP), 2022, pp. 2–36. URL: https://www.etsi.org/deliver/

etsi_tr/137900_137999/13790105/16.08.00_60/tr_13790105v160800p.pdf.

[38] John, P. Transmission Control Protocol. *RFC 793* (1981).